

Published in final edited form as:

Nature. 2021 January 01; 589(7842): 448–455. doi:10.1038/s41586-020-03046-1.

Fat1 deletion promotes hybrid EMT state, tumour stemness and metastasis

Ievgenia Pastushenko^{#1,2,3}, Federico Mauri^{#1}, Yura Song¹, Florian de Cock¹, Bob Meeusen^{4,5}, Benjamin Swedlund¹, Francis Impens^{6,7,8}, Delphi Van Haver^{6,7,8}, Matthieu Opitz⁹, Manuel Thery^{10,11}, Yacine Bareche¹², Gaele Lapouge¹, Marjorie Vermeersch¹³, Yves-Rémi Van Eycke^{14,15}, Cédric Balsat¹⁴, Christine Decaestecker^{14,15}, Youri Sokolow¹⁶, Sergio Hassid¹⁷, Alicia Perez-Bustillo¹⁸, Beatriz Agreda-Moreno¹⁹, Luis Rios-Buceta^{20,21,22}, Pedro Jaen^{20,21,22}, Pedro Redondo²³, Ramon Sieira-Gil²⁴, Jose F. Millan-Cayetano²⁵, Onofre Sanmatrin²⁶, Nicky D'Haene²⁷, Virginie Moers¹, Milena Rozzi¹, Jeremy Blondeau¹, Sophie Lemaire¹, Samuel Scozzaro¹, Veerle Janssens^{4,5}, Magdalena De Troya²⁵, Christine Dubois¹, David Pérez-Morga^{13,28}, Isabelle Salmon²⁷, Christos Sotiriou¹², Francoise Helmbacher²⁹, Cédric Blanpain^{1,30}

¹Laboratory of Stem Cells and Cancer, Université Libre de Bruxelles (ULB), Brussels, Belgium

²Dermatology Department, Cliniques de l'Europe, Brussels, Belgium

³Dermatology Department, CHU Brugmann, Université Libre de Bruxelles (ULB), Brussels, Belgium

⁴Laboratory of Protein Phosphorylation and Proteomics, Department of Cellular and Molecular Medicine, KU Leuven, Leuven, Belgium

⁵Leuven Cancer Institute (LKI), Leuven, Belgium

⁶VIB Center for Medical Biotechnology, Ghent, Belgium

⁷VIB Proteomics Core, Ghent, Belgium

Correspondence to: Cédric Blanpain.

Correspondence and requests for materials should be addressed to C.B. Cedric.Blanpain@ulb.ac.be .

Author contributions I.P., F.M. and C. Blanpain designed the experiments and performed data analysis. I.P. and F.M. performed most of the biological experiments. F.H. generated *Fat1*-cKO mice and provided her expertise. Y. Song performed bioinformatic analysis. F.d.C. and B.S. helped to perform CRISPR experiments. B.M. and V.J. performed intratracheal AdenoCRE installation for lung cancer generation. F.I. and D.V.H. performed phosphoproteomic analysis. M.O. and M.T. performed stiffness experiments. M.V. and D.P.-M. performed electron microscopy imaging and analysis. F.I. and D.V.H. performed phosphoproteomic analysis. Y.B. and C.S. performed analysis of patient survival using the TCGA database. I.S., Y. Sokolow, S.H., A.P.-B., B.A.-M., L.R.-B., P.J., M.D.T., P.R., R.S.-G., N.D'H., J.F.M.-C. and O.S. provided human samples. C. Balsat, C. Decaestecker and Y.-R.V.E. performed staining and analysis of patient-derived xenograft samples. C. Dubois performed FACS. V.M., S.L., G.L., J.B., M.R. and S.S. performed immunostainings, western blotting, treatments and follow-up of the mice. All authors read and approved the final manuscript.

Competing interests C. Blanpain, I.P. and F.M. are co-inventors on a patent application on the use of SRC inhibitors for the treatment of *FAT1*-mutated cancers.

Publisher's note Springer Nature remains neutral with regard to jurisdictional claims in published maps and institutional affiliations.

Reporting summary

Further information on research design is available in the Nature Research Reporting Summary linked to this paper.

Peer review information Nature thanks Salvador Aznar Benitah and the other, anonymous, reviewer(s) for their contribution to the peer review of this work.

Reprints and permissions information is available at <http://www.nature.com/reprints>.

- ⁸Department of Biomolecular Medicine, Ghent University, Ghent, Belgium
- ⁹Alvéole, Paris, France
- ¹⁰CytoMorpho Lab, UMR976 HIPI, CEA, INSERM, Université de Paris, Paris, France
- ¹¹CytoMorpho Lab, UMR5168 LPCV, CEA, CNRS, Université Grenoble-Alpes, Grenoble, France
- ¹²Breast Cancer Translational Research Laboratory J.-C. Heuson, Institut Jules Bordet, Université Libre de Bruxelles (ULB), Brussels, Belgium
- ¹³Center for Microscopy and Molecular Imaging (CMMI), Université Libre de Bruxelles (ULB), Charleroi, Belgium
- ¹⁴DIAPath, Center for Microscopy and Molecular Imaging, Université Libre de Bruxelles (ULB), Charleroi, Belgium
- ¹⁵Laboratory of Image Synthesis and Analysis, Ecole Polytechnique de Bruxelles, Université Libre de Bruxelles (ULB), Brussels, Belgium
- ¹⁶Department of Thoracic Surgery, Erasme University Hospital, Université Libre de Bruxelles (ULB), Brussels, Belgium
- ¹⁷Department of Otolaryngology – Head and Neck Surgery, Erasme University Hospital, Université Libre de Bruxelles (ULB), Brussels, Belgium
- ¹⁸Department of Dermatology, Complejo Asistencial Universitario de León, León, Spain
- ¹⁹Department of Otolaryngology – Head and Neck Surgery, Hospital Clínico ‘Lozano Blesa’, Zaragoza, Spain
- ²⁰Dermatology Department, Ramón y Cajal Hospital, Madrid, Spain
- ²¹University of Alcalá, Madrid, Spain
- ²²Instituto Ramón y Cajal de Investigación Sanitaria (IRyCIS), Madrid, Spain
- ²³Department of Dermatology, Clínica Universidad de Navarra, Navarra, Spain
- ²⁴Department of Maxillofacial Surgery, Head and Neck Surgery, Hospital Clínic, Barcelona, Spain
- ²⁵Department of Dermatology, Hospital Costa del Sol, Marbella, Spain
- ²⁶Department of Dermatology, Instituto Valenciano de Oncología, Valencia, Spain
- ²⁷Pathology Department, Erasme Hospital, Université Libre de Bruxelles (ULB), Brussels, Belgium
- ²⁸Laboratory of Molecular Parasitology, IBMM, Université Libre de Bruxelles (ULB), Charleroi, Belgium
- ²⁹Aix-Marseille Univ, CNRS, IBDM - UMR, 7288, Marseille, France
- ³⁰WELBIO, Université Libre de Bruxelles (ULB), Brussels, Belgium
- # These authors contributed equally to this work.

Abstract

FAT1, which encodes a protocadherin, is one of the most frequently mutated genes in human cancers^{1–5}. However, the role and the molecular mechanisms by which *FAT1* mutations control tumour initiation and progression are poorly understood. Here, using mouse models of skin squamous cell carcinoma and lung tumours, we found that deletion of *Fat1* accelerates tumour initiation and malignant progression and promotes a hybrid epithelial-to-mesenchymal transition (EMT) phenotype. We also found this hybrid EMT state in *FAT1*-mutated human squamous cell carcinomas. Skin squamous cell carcinomas in which *Fat1* was deleted presented increased tumour stemness and spontaneous metastasis. We performed transcriptional and chromatin profiling combined with proteomic analyses and mechanistic studies, which revealed that loss of function of *FAT1* activates a CAMK2–CD44–SRC axis that promotes YAP1 nuclear translocation and *ZEB1* expression that stimulates the mesenchymal state. This loss of function also inactivates EZH2, promoting *SOX2* expression, which sustains the epithelial state. Our comprehensive analysis identified drug resistance and vulnerabilities in *FAT1*-deficient tumours, which have important implications for cancer therapy. Our studies reveal that, in mouse and human squamous cell carcinoma, loss of function of *FAT1* promotes tumour initiation, progression, invasiveness, stemness and metastasis through the induction of a hybrid EMT state.

FAT1 is very frequently mutated in a broad range of human cancers—in particular, in squamous cell carcinomas (SCCs)^{1–5}. Mutations in *FAT1* have previously been associated with poor clinical outcome and resistance to anti-cancer therapy⁶. In skin SCCs induced by the chemical carcinogen 7,12-dimethylbenz[a]anthracene (DMBA) in combination with 12-*O*-tetradecanoylphorbol-13-acetate (TPA) (hereafter, DMBA/TPA), *Fat1* is mutated in about 20% of cases⁷, as in human SCCs. Stop-gain mutations are very frequently found, which indicates that these mutations result in loss of function (LOF) and that *FAT1* acts as a tumour-suppressor gene^{1,4,8}. Knockdown of *FAT1* using short hairpin RNA in human cancer cell lines has previously been shown to decrease cell–cell adhesion and promote cell migration, whereas contradictory results have been obtained regarding the role of *FAT1* in regulating EMT in vitro^{9,10}. However, a formal in vivo demonstration by a genetic LOF experiment that shows that *Fat1* acts as a tumour-suppressor gene is lacking. More importantly, the molecular mechanisms by which mutations in *FAT1* promote tumorigenesis and control tumour heterogeneity in vivo are completely unknown.

***Fat1* deletion promotes malignant progression**

To assess whether *Fat1* LOF promotes tumour initiation, we performed conditional deletion of *Fat1* in the skin epidermis using the constitutive *Krt14-cre* (*Krt14-cre;Fat1^{flox/flox};Rosa26^{YFP/+}*; hereafter referred to as *Fat1*-constitutive knockout (*Fat1*-cKO)) mouse model. *Fat1*-cKO mice were born at a Mendelian ratio and did not present skin abnormalities (Extended Data Fig. 1). Following administration of DMBA/TPA, tumorigenesis developed more rapidly: the number of benign and malignant tumours per mouse was increased in *Fat1*-cKO mice, which demonstrates that *Fat1* acts a tumour-suppressor gene in DMBA/TPA-induced skin SCCs (Extended Data Fig. 2a–f). To assess the role of *FAT1* in regulating malignant progression, we performed acute deletion of *Fat1* in benign papillomas using inducible *Krt14-creER* (*Krt14-creER; Fat1^{flox/flox};Rosa26^{YFP/+}*). Immunostaining and electron microscopy analyses revealed that after deletion of *Fat1*, the

polarity of the basal cells as well as the adherens and tight junctions were rapidly lost, the basal lamina became discontinued, the hemidesmosomes were decreased and KRT10 expression—characteristic of benign tumour differentiation—was rapidly lost (Extended Data Fig. 2j–r).

These data demonstrate that *Fat1* deletion promotes malignant progression by controlling cell polarity and adhesion between tumour cells, and between tumour cells and the extracellular matrix.

***Fat1* deletion promotes a hybrid EMT**

The histological differences we observed in benign papillomas persisted in malignant SCCs. *Fat1*-cKO tumour cells were less cohesive and had rounded shapes; most of these tumour cells expressed the mesenchymal marker vimentin, which suggest that they underwent EMT. Fluorescence-activated cell sorting (FACS) analysis showed that *Fat1*-cKO SCCs contained a large proportion of EPCAM⁺ cells, which was very rare in DMBA/TPA-induced SCCs with wild-type *Fat1*. The EMT occurred very early during tumour progression, as EPCAM⁺ tumour cells could be detected in papillomas (Fig. 1a–c, Extended Data Fig. 3).

Distinct tumour EMT states—which are characterized by the expression of different levels of the cell-surface markers EPCAM, CD106, CD61 and CD51, and represent different stages within the EMT process—have recently been recognized¹¹. The majority of the *Fat1*-cKO EPCAM⁺ EMT tumour cells were negative for the CD106, CD61 and CD51 markers or expressed CD106 alone; these represent two hybrid EMT subpopulations characterized by the co-expression of epithelial and mesenchymal markers in genetically induced skin SCCs¹¹. We performed cytospin on FACS-isolated tumour cells, which confirmed that *Fat1* deletion promoted the appearance of hybrid EMT subpopulations that co-express epithelial (KRT14) and mesenchymal (vimentin) markers (Fig. 1c–f). These data demonstrate that a genetic mutation in a tumour-suppressor gene can promote the acquisition of a hybrid EMT phenotype.

To assess whether *Fat1* LOF promotes the acquisition of a hybrid EMT phenotype in other models, we combined deletion of *Fat1* and *p53* (also known as *Trp53*) with *Kras*^{G12D} expression in different epidermal lineages. *Krt14-creER*, which targets the interfollicular epidermis, induces SCCs with well-differentiated phenotypes without EMT features, whereas *Lgr5-creER*—which targets the hair follicle—induces heterogeneous tumours characterized by different degrees of EMT¹². Similar to what we found in DMBA/TPA-derived SCCs, loss of *Fat1* in the *Krt14-creER;Kras*^{G12D};*p53*^{cKO};*Fat1*^{cKO};*Rosa26*^{YFP/+} mouse model promoted the acquisition of a hybrid EMT phenotype, whereas *Lgr5-creER*-induced SCCs—which presented high proportion of EMT phenotypes independently of *Fat1* deletion—did not further increase EMT features upon *Fat1* LOF. By contrast with the control condition¹¹, most *Lgr5-creER Fat1*-cKO tumour cells continued to express KRT14 and presented signs of squamous differentiation that were visible as keratin pearls (Extended Data Fig. 4a–m). These data demonstrate that, in three independent mouse models of skin SCC, *Fat1* deletion promotes the acquisition of stable hybrid EMT phenotypes.

To assess whether the promotion of the tumour hybrid state by *Fat1* deletion is skin-specific or whether it is conserved across different types of tumour, we combined *Fat1* and *p53* deletion with *Kras*^{G12D} expression in the lung epithelia by intratracheal instillation of *cre*-expressing adenovirus. *Fat1* deletion considerably increased the number of tumours per lung (Extended Data Fig. 4n, o), and these tumours also presented signs of hybrid EMT. Whereas *Kras*^{G12D} expression and *p53* deletion promoted the onset of adenocarcinomas characterized by expression of NKX2-1 (also known as TTF1), the simultaneous deletion of *Fat1* promoted the formation of lung SCCs, which were characterized by a decreased expression of NKX2-1 as well as by SOX2 expression (Fig. 1g–l). This is consistent with the higher proportion of *FAT1* mutations found in lung SCCs relative other types of lung cancer^{1,2}, and suggests that *FAT1* mutations could be a driving force for the squamous tumour phenotype.

To assess the human relevance of our findings, we performed *FAT1* deletion using CRISPR–Cas9 in the A388 human epithelial SCC cell line, which contains wild-type *FAT1*. Upon *FAT1* deletion, cells were less cohesive and more rounded, had decreased expression of E-cadherin and co-expressed epithelial (KRT14, p63 and SOX2) and mesenchymal (vimentin and ZEB1) markers (Fig. 1m), which is reminiscent of the EMT hybrid state found in mouse SCCs. By sequencing patient-derived xenotransplants of SCCs from different organs, we identified SCCs with and without *FAT1* LOF mutations. Co-immunostaining of pan-cytokeratin and vimentin showed that *FAT1*-mutated SCCs exhibit a much higher EMT hybrid score as compared to SCCs with wild-type *FAT1* (Fig. 1n, o, Extended Data Fig. 5). These data show that *FAT1* mutations promote the acquisition of a hybrid EMT state in human cancers.

***FAT1* deletion promotes stemness and metastasis**

EMT has previously been associated with an increase in tumour stemness^{11–14}. Tumour transplantation assays of *Fat1*-cKO and wild-type EPCAM⁺ and EPCAM⁻ tumour cells showed that *Fat1* LOF was associated with a tenfold increase in tumour-propagating cells as compared to *Fat1* wild type. The histology of the secondary tumours recapitulated the histology of the primary tumours (Fig. 2a, b). Tumour stemness is also associated with increased clonogenicity in vitro. To validate our findings, we assessed the clonogenicity of wild-type and *FAT1*-knockout human SCC cell lines in 3D tumour spheroid assays. *FAT1*-knockout cell lines grew much better than the isogenic wild-type control cell line (Fig. 2c, d). Altogether, these data show that *FAT1* deletion promotes tumour stemness in mouse and human cancers.

The hybrid EMT tumour state has previously been associated with the presence of circulating tumour cells and with increased metastatic potential upon intravenous injection of tumour cells¹¹. Notably, the proportion of the mice presenting lymph node and lung metastases and the number of metastases per mouse were increased in *Fat1*-cKO mice (Fig. 2e–h). Intravenous injection of EPCAM⁺ *Fat1*-cKO tumour cells gave rise to a higher number of lung metastasis as compared to tumour cells with wild-type *Fat1* (Fig. 2i–l), which demonstrates that *Fat1* LOF greatly increases spontaneous metastasis and lung colonization in skin SCCs, independently of the number of primary tumours or the

occurrence of EMT. These data demonstrate that *Fat1*-LOF-induced hybrid EMT state promotes metastasis in vivo.

Gene signature of *Fat1*-mutated tumours

To investigate the molecular mechanisms by which *Fat1* LOF promotes the hybrid EMT state, we first assessed the transcriptional signature of *Fat1*-mutated tumour cells from mouse skin SCCs. RNA sequencing (RNA-seq) revealed that *Fat1*-cKO EPCAM⁺ tumour cells presented a strong upregulation of many well-known EMT markers—including *Vim*, *Snail1*, *Prrx1*, *Twist1*, *Zeb1* or *Zeb2*—and the expression of these genes was further upregulated in EPCAM⁻ *Fat1*-knockout tumour cells, which suggests that EPCAM⁺ *Fat1*-cKO tumour cells are transcriptionally primed to undergo EMT. In contrast to EPCAM⁻ tumour cells from *Lgr5-creER; Kras^{G12D}; p53^{cKO}*-derived SCCs that present full EMT, EPCAM⁻ *Fat1*-cKO tumour cells continued to express high levels of several epithelial genes (such as *Krt14*, *p63* and *Sox2*). The transcriptional signature of *Fat1*-cKO tumour cells significantly overlapped with the hybrid EMT signature obtained by RNA-seq of CD106⁻CD61⁻CD51⁻ hybrid EMT tumour cells from *Lgr5-creER; Kras^{G12D}; p53^{cKO}* SCCs and did not overlap significantly with the full EMT signature¹¹ (Fig. 3a, b, Extended Data Fig. 5f, g).

RNA-seq data from EPCAM⁺ and EPCAM⁻ *Fat1*-cKO lung cancer cells and from CRISPR-Cas9 *FAT1*-knockout human SCC cells showed that—in both cases—similar mesenchymal genes (including *ZEB1*, *ZEB2* and *VIM*) were upregulated following deletion of *FAT1*, uncovering a common gene signature associated with *FAT1* deletion across different tumour types and between mouse and human cancers. Importantly, we found that high expression of this common *FAT1*-mutated signature was associated with poor survival in patients with lung SCC (Fig. 3c–e).

YAP1 and SOX2 regulate the hybrid EMT

To define the changes in the chromatin landscape that are responsible for the hybrid EMT state that occurs after deletion of *Fat1*, we performed assay for transposase-accessible chromatin using sequencing (ATAC-seq) of FACS-isolated wild-type and *Fat1*-cKO EPCAM⁺ and EPCAM⁻ tumour cells. We identified enhancers within key EMT transcription factors (such as *Zeb1*, *Snail1* or *Twist2*) and other EMT markers (for example, *Vim* or *Col6a3*) that were more accessible in EPCAM⁺ *Fat1*-cKO tumour cells as compared to EPCAM⁺ wild-type cells, which potentially accounts for the epigenetic priming of tumour cells to undergo EMT upon *Fat1* deletion. By performing motif discovery in differentially accessible chromatin regions between wild-type and *Fat1*-mutated tumour cells, we identified *Ap1* (also known as *Jun*) and Tead transcription-factor motifs as being strongly enriched in the chromatin regions that are more open in *Fat1*-mutated tumour cells that also have increased expression of YAP1 (Fig. 3f, Extended Data Fig. 6), which suggests that the JUN and FOS family of transcription factors cooperates with other transcription factors—including those of the TEAD family—that relay the YAP1 pathway to the nucleus to prime the *Fat1*-mutated cancer cells to undergo the EMT in skin SCC in vivo⁸.

To identify the transcription factors that are responsible for the sustained expression of epithelial genes in EPCAM⁻ *Fat1*-cKO tumour cells, we performed motif discovery in the ATAC-seq peaks that were upregulated in EPCAM⁻ *Fat1*-cKO as compared to EPCAM⁻ control tumour cells from fully mesenchymal *Lgr5-creER;Kras^{G12D};p53^{cKO}* SCCs. We found that *Ap1*, *Sox* or *Klf* motifs were strongly enriched in EPCAM⁻ *Fat1*-cKO cells (Fig. 3g, Extended Data Fig. 6), which suggests that the epithelial program of the hybrid EMT state in *Fat1*-cKO is mediated by an AP1–SOX2–KLF transcriptional network. *SOX2* is amplified in many human SCCs and marks cancer stem cells in skin SCCs^{15–17}, and could be responsible for the sustained expression of epithelial genes in *Fat1*-cKO tumour cells.

To functionally validate the bioinformatic predictions, we assessed the effect of CRISPR–Cas9-mediated deletion of *Yap1* and *Taz*, or of *Sox2*, on tumour stemness, metastasis and the gene expression program of mouse skin SCCs. Both tumour-propagating cell frequency and the number of metastasis were reduced upon deletion of *Sox2* or of *Yap1* and *Taz* in primary EPCAM⁻ cell lines derived from *Lgr5-creER;Kras^{G12D};p53^{cKO};Fat^{cKO}* SCCs (Fig. 3h, i), which demonstrates that the SOX2 and the YAP1 and TAZ transcriptional programs are important for the promotion of tumour stemness and metastasis downstream of *Fat1* deletion. *SOX2* or *YAP1* deletion in the human SCC cell line decreased the tumour growth mediated by *FAT1* deletion in 3D spheroid assays (Fig. 3j), which demonstrates that SOX2 and YAP1 promote tumour growth downstream of *FAT1* deletion in human cancer cells. Conversely, the deletion of the E-cadherin gene (*CDH1*) in the same cell line—which induced defects of cell adhesion—did not induce SOX2 or ZEB1 expression, or an increase in nuclear YAP1. Overexpression of *CDH1* in *FAT1*-knockout cells did not decrease the clonogenicity or the expression of mesenchymal genes induced by *FAT1* deletion (Extended Data Fig. 7a–f), which shows that the promotion of tumour stemness or the hybrid EMT phenotype by *FAT1* deletion is not simply the result of a defect in cell adhesion.

Sox2 deletion in *Lgr5-creER;Kras^{G12D};p53^{cKO};Fat^{cKO}* SCCs resulted in the loss of epithelial characteristics and a shift from hybrid to complete EMT upon subcutaneous transplantation, whereas the deletion of *Yap1* and *Taz* promoted an early hybrid EMT state (as shown by immunostaining and FACS analysis) (Fig. 3k–m, Extended Data Fig. 7g–i). The RNA-seq data from *Fat1* and *Sox2* knockout further demonstrated a significant enrichment in the late EMT signature, marked by an increase of mesenchymal markers (for example, *Lox* and *Pdgfra*) and a decrease of epithelial markers (for example, *Cebpa*, *Krt5* and *p63*). Instead, the transcriptome of *Fat1*, *Yap1* and *Taz* triple-knockout SCCs showed significant enrichment of the EPCAM⁺ epithelial and early hybrid EMT signature. Many classical canonical target genes of YAP1 and TAZ (for example, *Ctgf* (also known as *Ccn2*), *Amotl2* and *Fstl1*), as well as EMT genes (for example, *Vcam1*, *Thy1* and *Pdgfrb*), were decreased after *Fat1*, *Yap1* and *Taz* triple knockout as compared to *Fat1* knockout (Fig. 3n, o, Extended Data Fig. 7j, k and data not shown). Altogether, these data demonstrate that SOX2, and YAP1 and TAZ, control distinct transcriptional programs that lead to a stable hybrid EMT phenotype downstream of *Fat1* LOF.

Signalling cascades downstream of *FAT1*

To understand how *FAT1* LOF activates SOX2 or YAP1 and TAZ, we performed a phosphoproteomic analysis of wild-type and CRISPR–Cas9 *FAT1*-knockout human SCC cells. We identified 288 phosphosites that were significantly upregulated and 335 that were significantly downregulated in *FAT1*-knockout tumour cells as compared to *FAT1* wild type. *FAT1* LOF induced a decrease in the phosphorylation of proteins involved in cell–cell adhesion (such as ZO1 or ZO2), as well as of PRKCD, EGFR, ERBB2, MEK1, MEK2, AKT2 or MTOR. In good accordance with the phosphoproteomic analysis, MEK1 and MEK2 were significantly less phosphorylated—and the total levels of EGFR and phosphorylated EGFR—were decreased in *FAT1*-knockout tumour cells (Fig. 4a–c, Extended Data Figs. 8, 9). These data suggest that EGFR–RAS–RAF–MEK–MAPK and the EGFR–PI3K–AKT–MTOR signalling pathways are decreased upon *FAT1* LOF.

Conversely, *FAT1*-deficient tumour cells exhibited a strong increase in the phosphorylation of the YES tyrosine kinase that belongs to the SRC family, as well as of the MAP1B and GJA1 proteins. GJA1 phosphorylation promotes GJA1 localization at the plasma membrane and increases the formation of functional gap junctions, which has previously been linked to increased metastatic capacity¹⁸ (Extended Data Fig. 8). These data suggest that *FAT1* LOF induces a global remodelling of cell–cell adhesions, cell communication and the cytoskeleton, which is associated with the acquisition of a hybrid EMT state.

To decipher the signalling cascade that acts downstream of *FAT1* LOF, we used the PhosphoSitePlus online tool and bibliographic search to predict kinases that act upstream of the phosphosites we identified. Ca²⁺/calmodulin-dependent protein kinase II (CAMK2) was the kinase that we found to most frequently act upstream of phosphopeptides enriched in *FAT1*-knockout tumour cells (CD44 on S706¹⁹ and GJA1 on S328, S325, S306, S330, S364 and S365²⁰). In accordance with the bio-informatic prediction, western blot analysis showed that CAMK2 was substantially more phosphorylated in *FAT1* LOF as compared to *FAT1* wild type. We further confirmed that SRC and YES also showed high levels of expression and phosphorylation upon *FAT1* LOF. Immunoprecipitation of SRC and YES showed that YES was substantially more highly expressed and phosphorylated with *FAT1* knockout, whereas the levels of SRC were comparable between *FAT1* wild-type and -knockout tumour cells, and SRC phosphorylation was increased after *FAT1* knockout (Extended Data Fig. 8h). Treatment with a CAMK2 inhibitor (KN93) greatly decreased the level of SRC and YES phosphorylation, which shows that CAMK2 directly or indirectly phosphorylates YES and SRC upon *FAT1* LOF (Fig. 4d–f, Extended Data Fig. 8).

CD44 is upregulated during EMT, promoting tumour stemness, progression and metastasis²¹. Previous computational analysis predicted that an ESRP1–CD44–ZEB1 loop stabilizes the hybrid EMT state in human lung cancer cells²². Phosphorylation of CD44 by different kinases, including CAMK2²³, regulates its cellular localization and activity. To assess whether CD44 phosphorylation at S706 (which is upregulated upon *FAT1* LOF) could affect CD44 cellular localization, we performed a FACS analysis that revealed increased levels of cell-surface CD44 in *FAT1*-knockout cells, which were significantly reduced upon treatment with a CAMK2 inhibitor (Fig. 4g–i). To determine whether CAMK2

phosphorylates YES and SRC directly or through CD44²¹ signalling in *FAT1*-knockout cells, we performed *CD44* deletion using CRISPR–Cas9 in *FAT1*-knockout cells and found that phosphorylation of SRC was decreased upon double knockout of *CD44* and *FAT1* (Fig. 4g–j). These data demonstrate that upon *FAT1* LOF, CAMK2 activates SRC at least partially through CD44. The clonogenicity of *FAT1* and *CD44* double-knockout human SCC cells decreased significantly in 3D tumour spheroid assays (Fig. 4k), which demonstrates that CD44 stabilization contributes to the increase in tumour stemness observed upon *FAT1* LOF.

We further assessed whether the hybrid EMT phenotype could be promoted by CAMK2–CD44–SRC signalling. We found that *FAT1* and *CD44* double-knockout and *FAT1*-knockout cells treated with CAMK2 (KN93) or SRC (saracatinib or dasatinib) inhibitors presented a strong decrease in nuclear YAP1 and ZEB1 and an increase in expression of E-cadherin, and were growing in more-compact epithelial colonies. These results demonstrate that *FAT1* LOF activates a CAMK2–CD44–SRC–YAP–ZEB1 axis that promotes the expression of a mesenchymal program. We observed a decrease in SOX2 expression only in *FAT1*-knockout tumour cells treated with a CAMK2 inhibitor. However, no change in SOX2 expression was observed upon inhibition of the CD44–SRC cascade (Fig. 4l).

Phosphoproteomic analysis revealed an increase in the inactivating phosphorylation of EZH2 at T487²⁴ in *FAT1*-knockout cells. EZH2 belongs to the PRC2 complex that methylates H3 at K27, mediating transcriptional repression²⁵. This histone mark is remodelled at the *Sox2* locus during the formation of SCCs¹⁵. We hypothesized that EZH2 inhibition in *FAT1*-knockout cells could decrease trimethylation of H3 at K27 (H3K27me3) repressive histone marks, and thus promote the expression of *SOX2*. The global level of H3K27me3 was substantially decreased in *FAT1*-knockout cells, which suggests that EZH2 could be less active upon *FAT1* LOF. Administration of a CAMK2 inhibitor increased the global levels of H3K27me3 in *FAT1*-knockout cells, consistent with the notion that CAMK2 activation inhibits EZH2 and PRC2 activity in tumour cells. To further validate this hypothesis, we treated *FAT1* wild-type cells with an EZH2 inhibitor (GSK343) and observed a decrease of H3K27me3 and increase in *SOX2* mRNA and protein expression after seven days of treatment, which further suggests that *SOX2* is epigenetically regulated by a *FAT1*–CAMK2–EZH2-dependent mechanism. Chromatin immunoprecipitation with quantitative PCR (ChIP–qPCR) demonstrated that H3K27me3 marks around the *SOX2* promoter were significantly reduced upon *FAT1* deletion, which provides support for the notion that *FAT1* deletion regulates the expression of *SOX2* through an epigenetic mechanism (Fig. 4m–r).

As YAP1 and TAZ signalling can be regulated by the stiffness of the extracellular matrix²⁶, we assessed the effect of substrate stiffness on YAP1 and *SOX2* expression. In contrast to *FAT1* wild-type cells, *FAT1*-knockout tumour cells exhibited high levels of total and nuclear YAP1 expression even on a soft substrate, which demonstrates that *FAT1* deletion constitutively activates signalling pathways that lead to high YAP1 expression; this causes the *FAT1*-knockout cells to behave—in respect to YAP1 nuclear expression—as if the tumour cells were exposed to a stiff substrate. No changes in *SOX2* expression were observed, demonstrating that *SOX2* is constitutively activated upon *FAT1* LOF independently of the extracellular stiffness (Extended Data Fig. 10a–d).

Drug vulnerabilities in *FAT1*-mutated tumours

To test whether the signalling cascades that change upon *FAT1* LOF could predict therapeutic resistance and vulnerability of *FAT1*-mutated cancers, we assessed the sensitivity of wild-type and isogenic *FAT1*-knockout human cancer cell lines to the inhibitors of the signalling pathways that we found to be differentially regulated between wild-type and *FAT1*-knockout cells. EGFR inhibitors such as afatinib, and MEK inhibitors such as trametinib, are widely used in patients with metastatic SCC^{27,28}. *FAT1*-knockout cells were significantly more resistant to afatinib and trametinib as compared to *FAT1* wild-type SCC cells in vitro (Fig. 4s–u).

By contrast, *FAT1*-knockout tumour cells were significantly more sensitive to the SRC inhibitors dasatinib and saracatinib and the CAMK2 inhibitor KN93 as compared to *FAT1* wild-type tumour cells (Fig. 4s–u). Administration of afatinib and dasatinib to mice transplanted with *FAT1* wild-type and -knockout human SCC cell lines showed that *FAT1* wild-type tumour cells were more sensitive to afatinib and *FAT1*-knockout tumour cells were more sensitive to dasatinib (Fig. 4v, w), consistent with the difference in drug sensitivity observed in vitro.

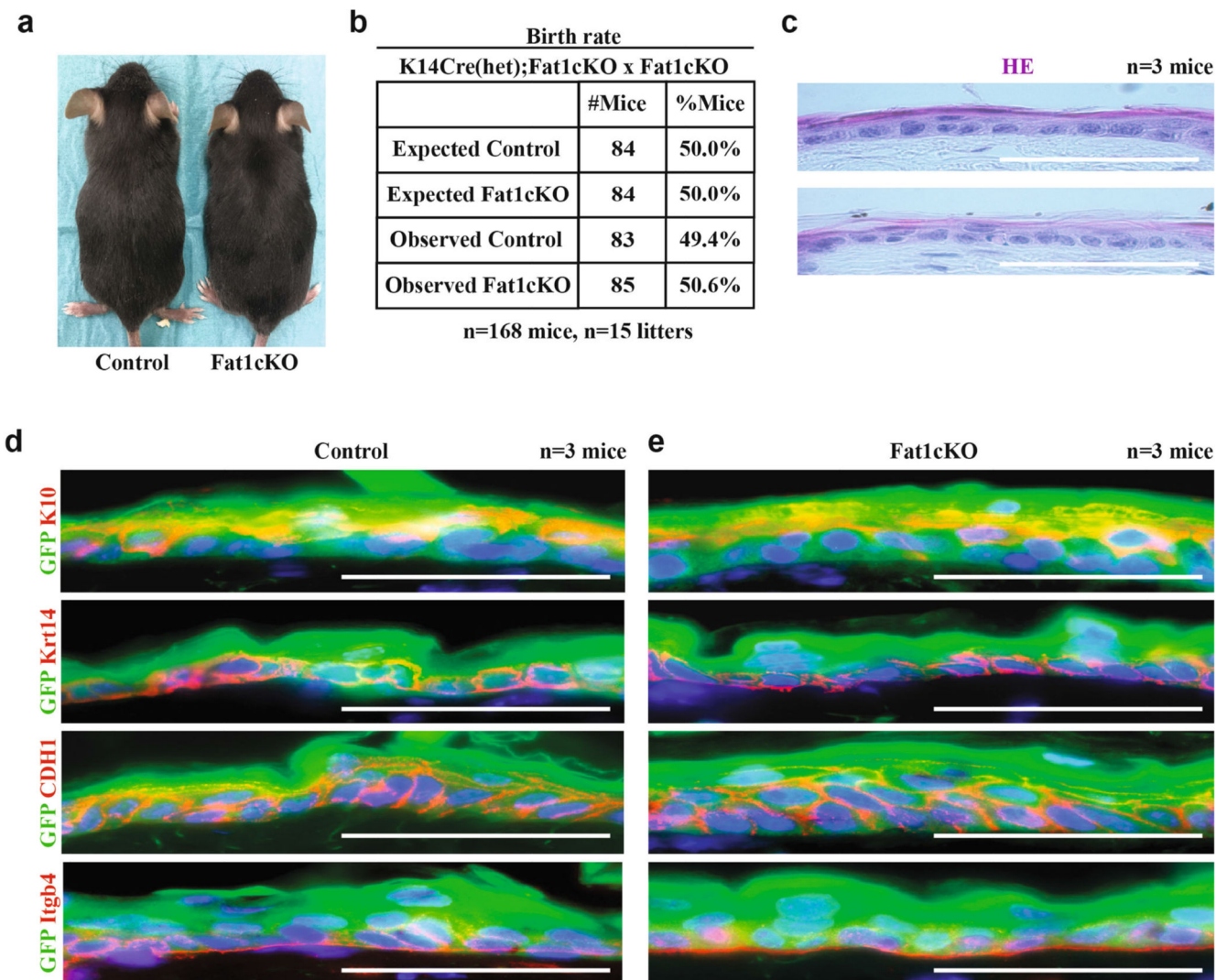
Discussion

Our study reveals that, in mouse models and human cancers, *FAT1* deletion promotes the acquisition of a hybrid EMT state that presents increased tumour stemness and metastasis. We identify the epigenetic and transcriptional mechanisms that link a loss of cell polarity and cell adhesion with the induction of a hybrid EMT phenotype downstream of *Fat1* deletion. Our comprehensive molecular characterization—including transcriptomic, epigenomic and proteomic characterization of *Fat1* mutants—shows that the hybrid EMT signature is mediated by the activation of YAP1 and SOX2, which regulate the co-expression of mesenchymal and epithelial transcriptional programs, respectively, in cancer cells. We show that the gene signature associated with *FAT1* LOF is predictive of poor survival in patients with lung cancer. We identify the signalling cascades that lead to the activation of YAP1 and SOX2 downstream of *FAT1* LOF. The activation and inhibition of these signalling pathways lead to an increased sensitivity of *FAT1*-mutated cancer cells to CAMK2 and SRC inhibition and to resistance to EGFR and MEK inhibition (Extended Data Fig. 10). This study has important implications for personalized medicine, in the prognosis and treatment of the high number of patients with cancer that displays *FAT1* mutations.

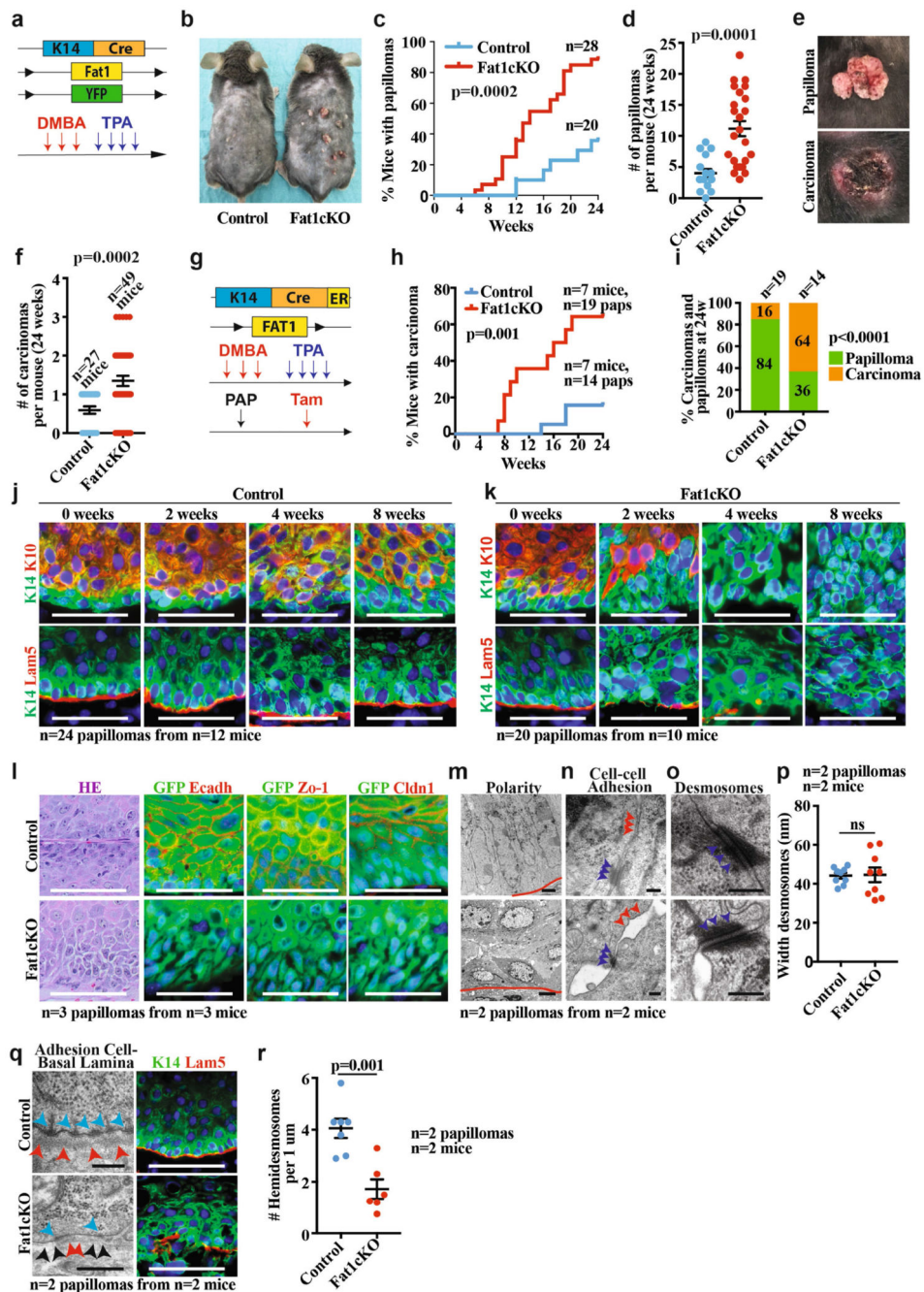
Online content

Any methods, additional references, Nature Research reporting summaries, source data, extended data, supplementary information, acknowledgements, peer review information; details of author contributions and competing interests; and statements of data and code availability are available at <https://doi.org/10.1038/s41586-020-03046-1>.

Extended Data

**Extended Data Fig. 1. *Fat1* LOF does not alter development and skin homeostasis.**

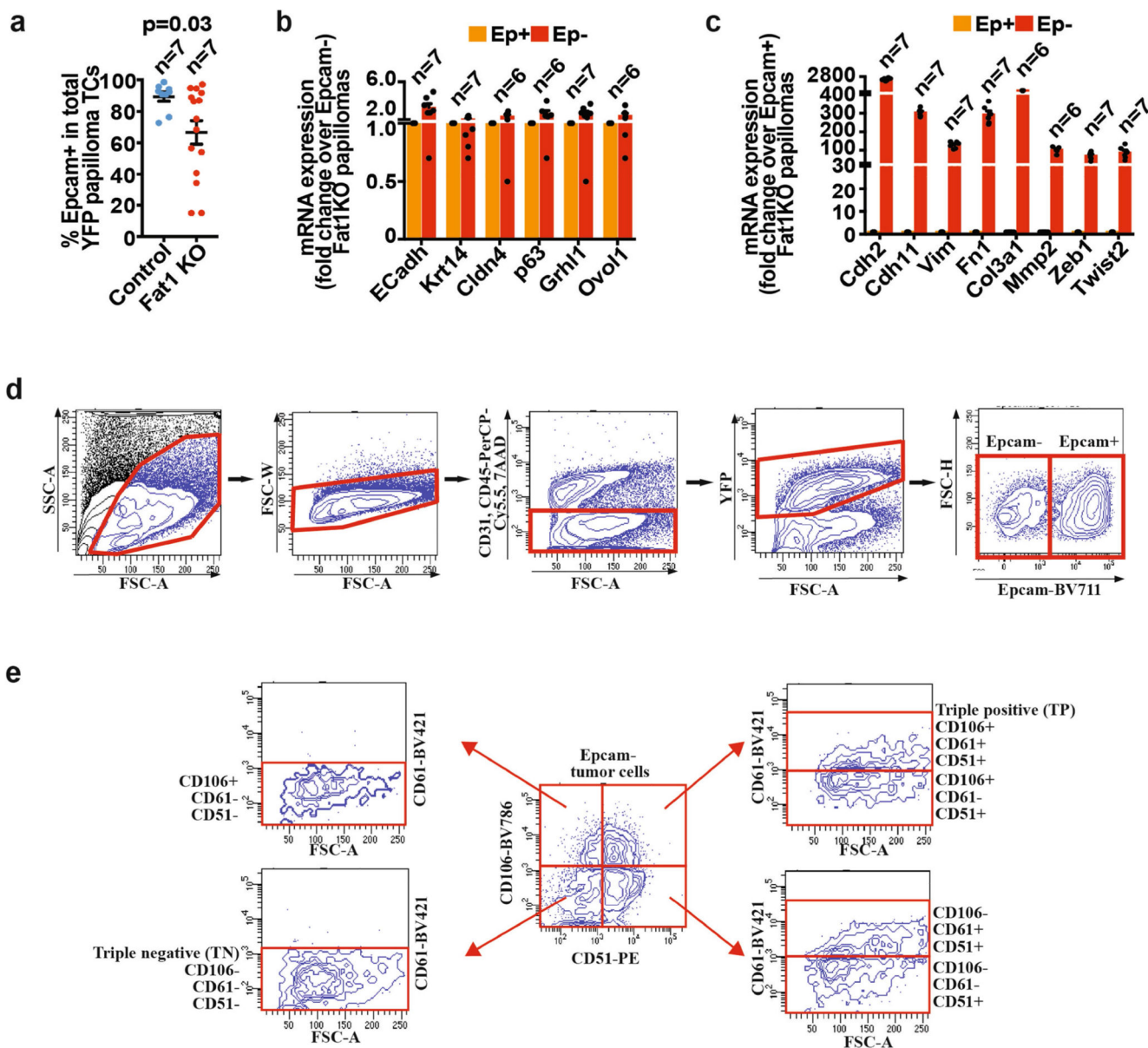
a, Image showing *Fat1*-cKO mouse and its control littermate. **b**, Table showing the number of control mice and mice with constitutive *Fat1*-cKO in skin epidermis, showing the absence of deviation from Mendelian ratio. **c**, Haematoxylin and eosin staining in control and *Fat1*-cKO epidermis. Scale bar, 50 μ m. **d**, **e**, Immunostaining for GFP and KRT10, KRT14, E-cadherin or ITGB4 in control (**d**) and *Fat1*-cKO (**e**) epidermis. Scale bar, 50 μ m.



Extended Data Fig. 2. *Fat1* LOF accelerates DMBA/TPA-induced tumour initiation and malignant progression.

a, Model allowing constitutive *Fat1* deletion in the skin epidermis and the scheme of DMBA/TPA protocol. **b**, Control and *Fat1*-cKO littermates 24 weeks after initiation of DMBA/TPA treatment. **c**, **d**, Time elapsed from the beginning of DMBA/TPA treatment until the appearance of the tumour (log-rank Mantel–Cox test) (**c**) and the number of papillomas per mouse (mean ± s.e.m., two-tailed *t*-test) (**d**) in control and *Fat1*-cKO mice. **e**, Macroscopic appearance of papilloma and carcinoma. **f**, Number of carcinomas per

mouse at 24 weeks after DMBA/TPA in control and *Fat1*-knockout mice. Mean \pm s.e.m., two-tailed *t*-test. **g**, Acute deletion of *Fat1* in DMBA/TPA-induced papillomas. **h**, Time elapsed from tamoxifen (tam) administration to macroscopic malignant progression from papillomas into carcinomas. log-rank Mantel–Cox test. **i**, Proportion of papillomas that progressed to carcinomas in control and *Fat1*-cKO mice. χ^2 test. **j**, **k**, Immunostaining for KRT14, KRT10 and LAM5 in control (**j**) and *Fat1*-cKO papillomas (**k**) 0, 2, 4 and 8 weeks after tamoxifen administration. Scale bar, 50 μ m. **l**, Haematoxylin and eosin and immunostaining for YFP, E-cadherin, ZO-1 or CLDN1 in control and *Fat1*-cKO papillomas. Scale bar, 50 μ m. **m–o**, Electron microscopy images showing polarity (Scale bars, 2 μ m (control papilloma), 5 μ m (*Fat1*-cKO papilloma)) (**m**), cell–cell adhesion (scale bar, 0.2 μ m) (**n**) or desmosomes (scale bar, 0.2 μ m) (**o**) in *Fat1*-cKO and wild-type papillomas. Red lines indicate interface between tumour cells and stroma. Blue arrowheads, desmosomes. Red arrowheads, tight and adherens junctions. **p**, Width of the desmosomes measured in nm in control and *Fat1*-cKO papillomas. Mean \pm s.e.m., two-tailed *t*-test. **q**, Electron microscopy (scale bars, 0.2 μ m (control), 5 μ m (*Fat1*-cKO)) and immunostaining for KRT14 and LAM5 (scale bar, 50 μ m) of control and *Fat1*-cKO papillomas. Blue arrowheads, hemidesmosomes. Red arrowheads, basal lamina in control papillomas and discontinued basal lamina in *Fat1*-cKO papillomas. Black arrowheads show fenestration of basal lamina in *Fat1*-cKO papillomas. **r**, Number of hemidesmosomes per 1 μ m. Mean \pm s.e.m., two-tailed *t*-test).



Extended Data Fig. 3. EMT in papillomas and gating strategy for FACS analysis and cell sorting of the tumour subpopulations.

a. Percentage of EPCAM⁺YFP⁺ tumour cells in control and *Fat1*-cKO papillomas.

Mean ± s.e.m., two-tailed *t*-test. **b, c,** mRNA (qPCR) expression of epithelial

(**b**) and mesenchymal (**c**) genes in EPCAM⁺ and EPCAM⁻ control and *Fat1*-

cKO papillomas. Mean + s.e.m. **d,** FACS plots showing the gating strategy

used to FACS-isolate or to analyse the proportion of YFP⁺EPCAM⁺ and

EPCAM⁻ tumour cells from DMBA/TPA-induced *K14-cre;Fat1^{cKO};Rosa26^{YFP/+}*

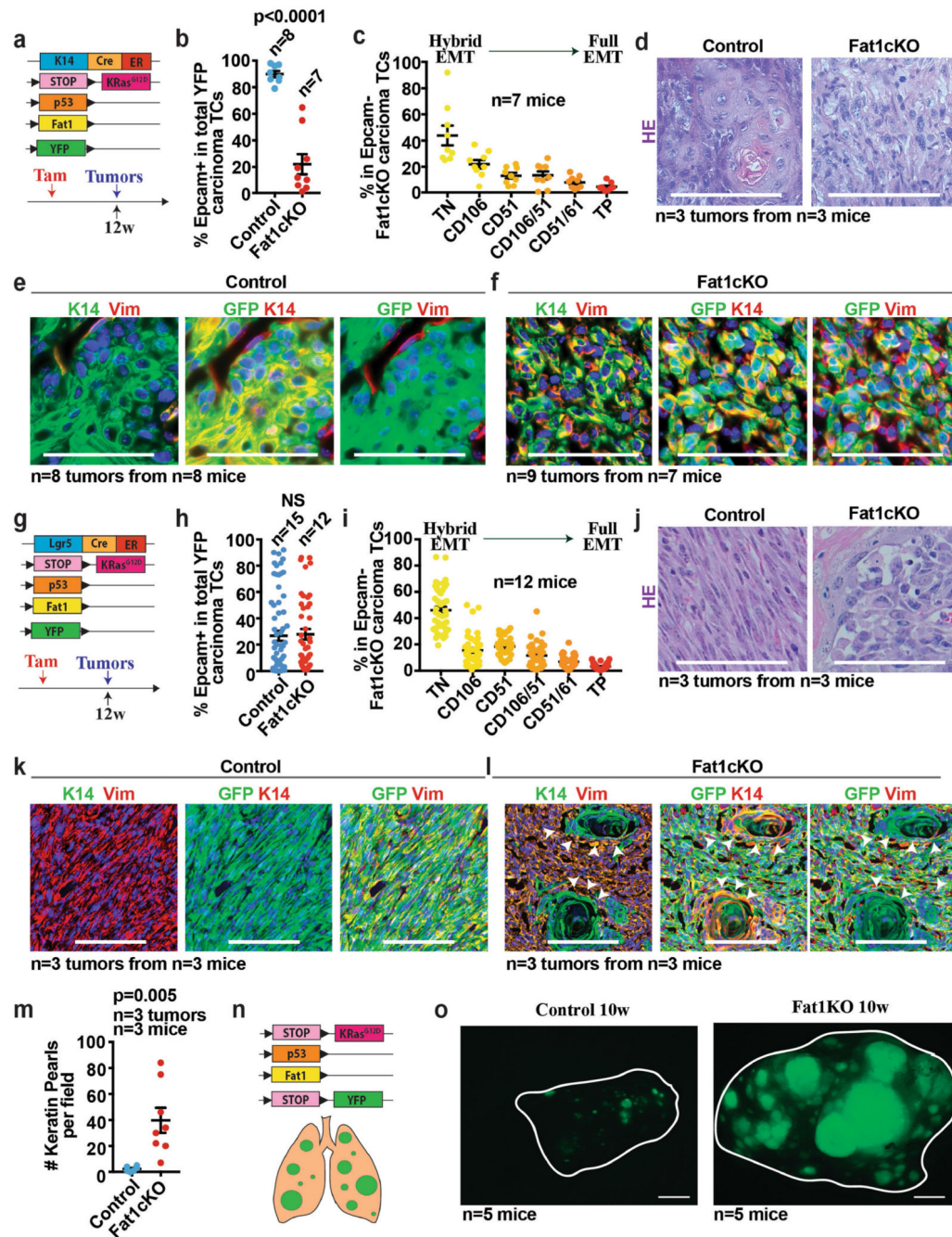
carcinomas and papillomas, *Lgr5-creER;KRas^{G12D};p53^{cKO};Fat1^{cKO};Rosa26^{YFP/+}*

or *K14-creER;KRas^{G12D};p53^{cKO};Fat1^{cKO};Rosa26^{YFP/+}* skin SCCs and

Kras^{G12D};p53^{cKO};Fat1^{cKO};Rosa26^{YFP/+} lung carcinomas. **e,** FACS

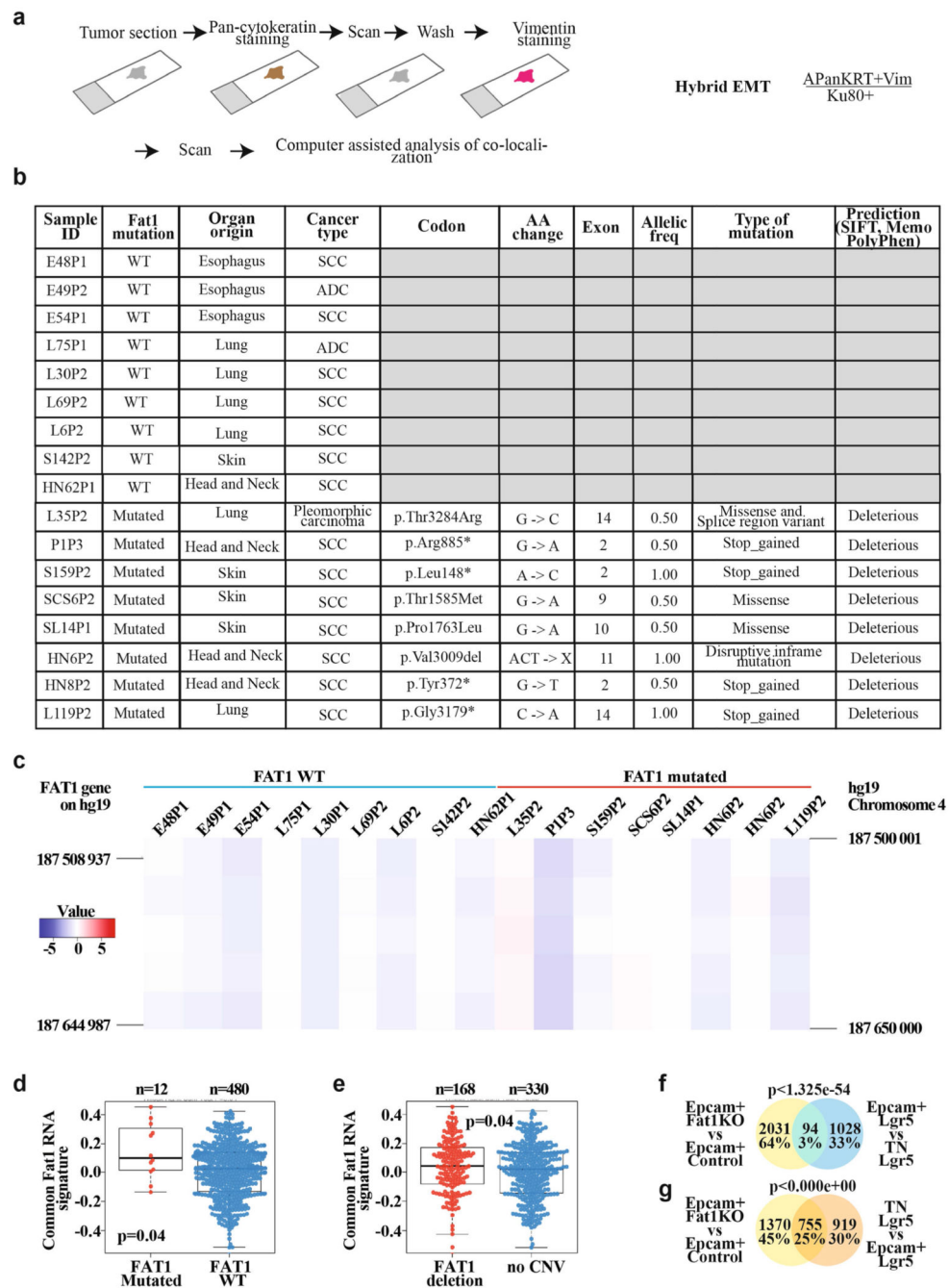
plots showing the gating strategy to define the six

subpopulations of EPCAM⁻ tumour cells: EPCAM⁻CD106⁻CD51⁻CD61⁻ (triple negative), EPCAM⁻CD106⁺CD51⁻CD61⁻, EPCAM⁻CD106⁻CD51⁺CD61⁻, EPCAM⁻CD106⁺CD51⁺CD61⁻, EPCAM⁻CD106⁻CD51⁺CD61⁺ and EPCAM⁻CD106⁺CD51⁺CD61⁺ (triple positive) populations.



Extended Data Fig. 4. *Fat1* LOF promotes hybrid EMT state in a genetic model of skin SCC. **a**, Mouse model of skin SCC allowing YFP and *Kras*^{G12D} expression as well as *p53* and *Fat1* deletion preferentially in the interfollicular epidermis (IFE) using *Krt14-creER*.

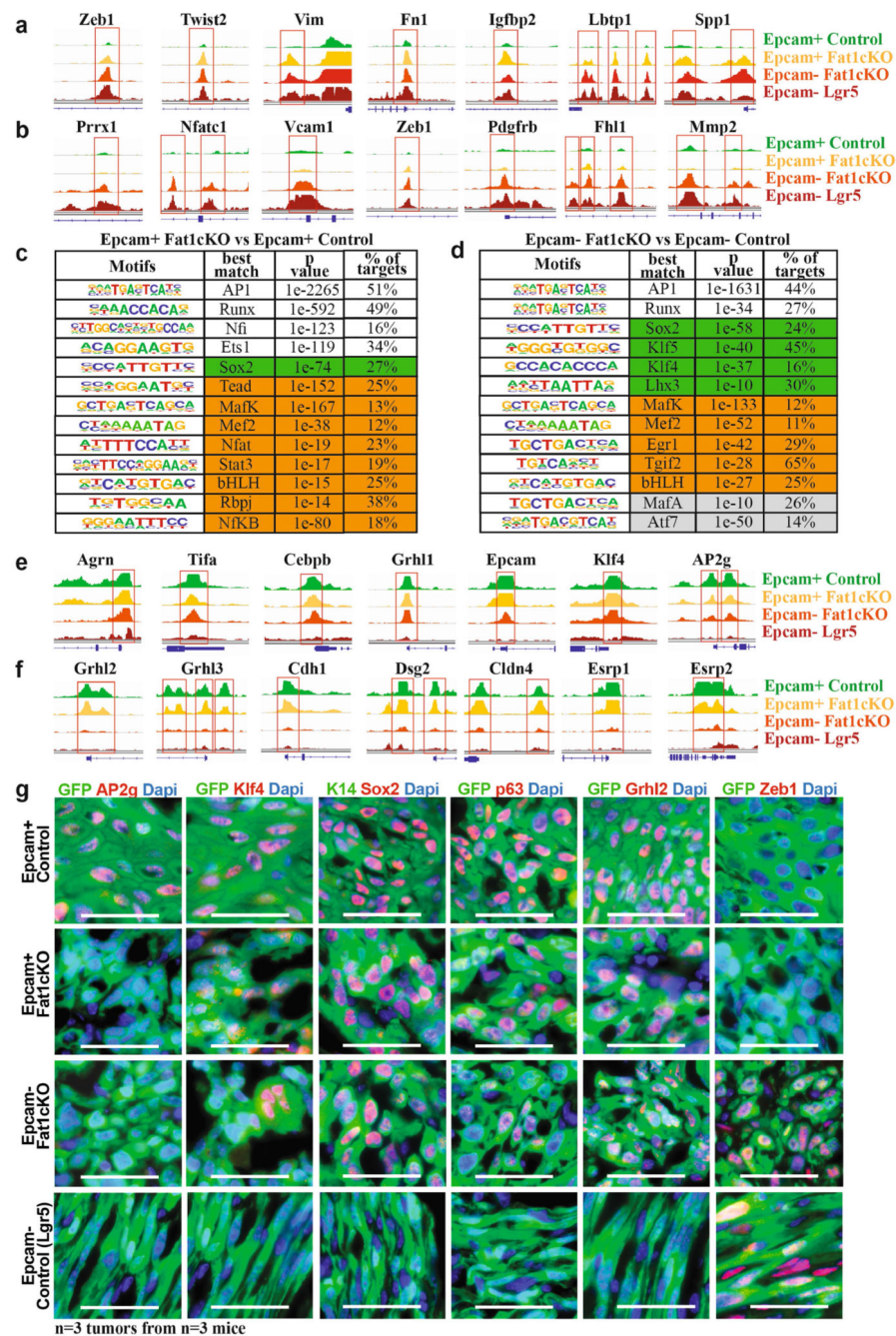
b, Percentage of EPCAM⁺ tumour cells in control and *Fat1*-cKO SCCs. Mean \pm s.e.m., two-tailed *t*-test. **c**, Graph showing the distribution of the different EPCAM⁻ tumour cell subpopulations on the basis of the expression of CD106/VCAM1, CD61/ITGB3 and CD51/ITGAV in *Fat1*-cKO tumours. Mean \pm s.e.m. **d**, Haematoxylin and eosin staining, showing representative control and *Fat1*-cKO tumours. Scale bar, 50 μ m. **e**, **f**, Immunostaining for GFP, KRT14 or vimentin in representative control (**e**) and *Fat1*-cKO tumour (**f**). Scale bar, 50 μ m. **g**, Mouse model of skin SCC allowing the expression of YFP and *Kras*^{G12D} as well as *p53* and *Fat1* deletion preferentially in the hair follicle lineage using *Lgr5-creER*. **h**, Percentage of EPCAM⁺ tumour cells in the control and *Fat1*-cKO tumours. Mean \pm s.e.m., two-tailed *t*-test. **i**, Graph showing the distribution of the different EPCAM⁻ tumour cell subpopulations on the basis of the expression of CD106/VCAM1, CD61/ITGB3 and CD51/ITGAV in *Fat1*-cKO tumours. Mean \pm s.e.m. **j**, Haematoxylin and eosin staining, showing a representative *Fat1* wild-type and *Fat1*-cKO tumour. Scale bar, 50 μ m. **k**, **l**, Immunostaining for KRT14 and vimentin showing the absence of keratin pearls in representative EPCAM⁻ control SCC (**k**) and the presence of keratin pearls in representative EPCAM⁻ *Fat1*-cKO SCC (**l**). White arrowheads indicate keratin pearls. Scale bar, 100 μ m. **m**, Dot plot showing the number of keratin pearls quantified per field at magnification 20 \times . *n* = 5 fields quantified per sample, mean \pm s.e.m., two-tailed *t*-test. **n**, Mouse model allowing YFP and *Kras*^{G12D} expression as well as *p53* and *Fat1* deletion in lung epithelial cells using intratracheal instillation of Ad5CMVCre virus. **o**, Immunofluorescence image showing the YFP⁺ lung tumours 10 weeks after intratracheal instillation of Ad5CMVCre virus in *Fat1* wild-type and *Fat1*-cKO mice. Scale bar, 1 mm.



Extended Data Fig. 5. Mutations in *FAT1* promotes hybrid EMT state in human cancers.

a, Schematic representing the method of analysing the co-expression of pan-cytokeratin and vimentin using immunohistochemistry of patient-derived xenografts that present (or not) mutations in *FAT1*, and the definition of hybrid EMT score. **b**, Table summarizing the samples of patient-derived xenografts on which whole-exome sequencing was performed, and detailed information on the mutations: codon, amino acid change, the exon containing the mutation, the allelic frequency, the type of mutations and the bioinformatic prediction of the effect of the mutation on the function of the protein using three bioinformatic algorithms

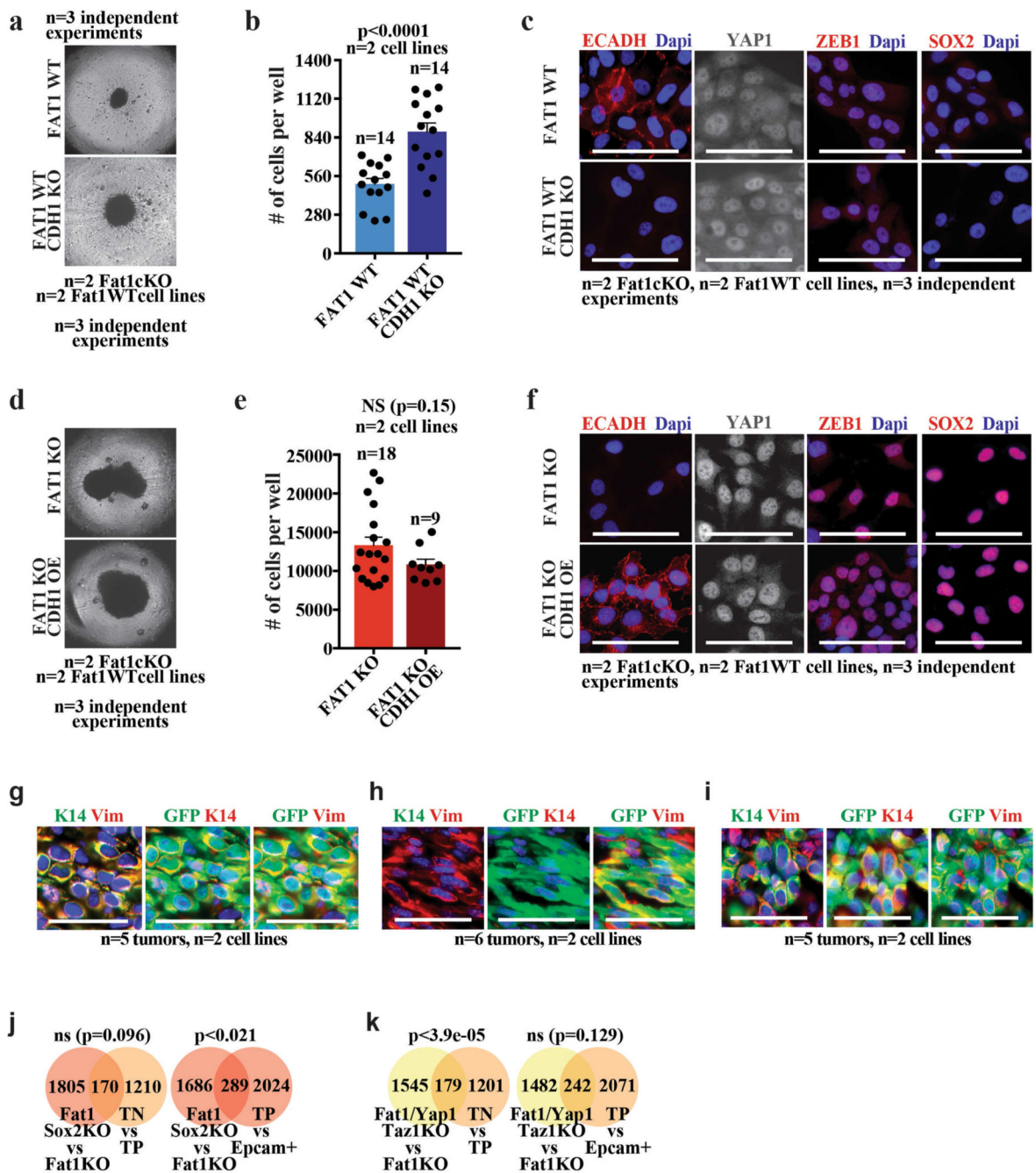
(SIFT, Memo and PolyPhen). **c**, Heat map showing the copy number variation profile of *FAT1* genomic region in the patient-derived xenograft samples included in the analysis of hybrid EMT score. The colour code corresponds to the quantified copy number and the genomic coordinate (reference genome hg19) of bin set for quantification. The *FAT1* gene is marked on each vertical edge. **d, e**, Box plot showing the distribution of the common mRNA signature (mouse skin and lung *Fat1*-cKO SCCs and human *FAT1*-knockout SCC cell line) compared to *FAT1* mutation status in human lung SCC (TCGA database; for the analysis, only high-impact mutations in >20% of variant allele frequency were considered) (**d**) and *FAT1* copy number variation status in human lung SCC (TCGA database) (**e**). Boundaries of the box indicate the first and third quartiles of the *FAT1* RNA signature value. The bold horizontal line indicates the median and the two external horizontal lines shows the minimum and maximum values. The dots represent all data points. Differences between the two groups are assessed using a two-sided Wilcoxon rank-sum test. **f, g**, Venn diagram of the genes upregulated in the EPCAM⁺ *Fat1*-cKO skin SCC and upregulated in LGR5 EPCAM⁺ versus triple-negative hybrid EMT tumour cells (**f**) or in triple-negative versus EPCAM⁺ cells (**g**). Two-sided hypergeometric test.



Extended Data Fig. 6. EPCAM⁺ *Fat1*-cKO tumour cells are epigenetically primed to undergo EMT, whereas EPCAM⁻ *Fat1*-cKO sustain the expression of epithelial program.

a. ATAC-seq profiles of the chromatin regulatory regions of mesenchymal genes closed in control EPCAM⁺ tumour cells and opened in EPCAM⁺ *Fat1*-cKO tumour cells, showing epigenetic priming of EPCAM⁺ *Fat1*-cKO tumour cells to undergo EMT. **b.** ATAC-seq profiles of the chromatin regulatory regions of mesenchymal genes with open chromatin regions only in EMT EPCAM⁻ tumour cells. **c.** Transcription factor motifs enriched in the ATAC-seq peaks upregulated between the EPCAM⁺ *Fat1*-cKO and EPCAM⁺

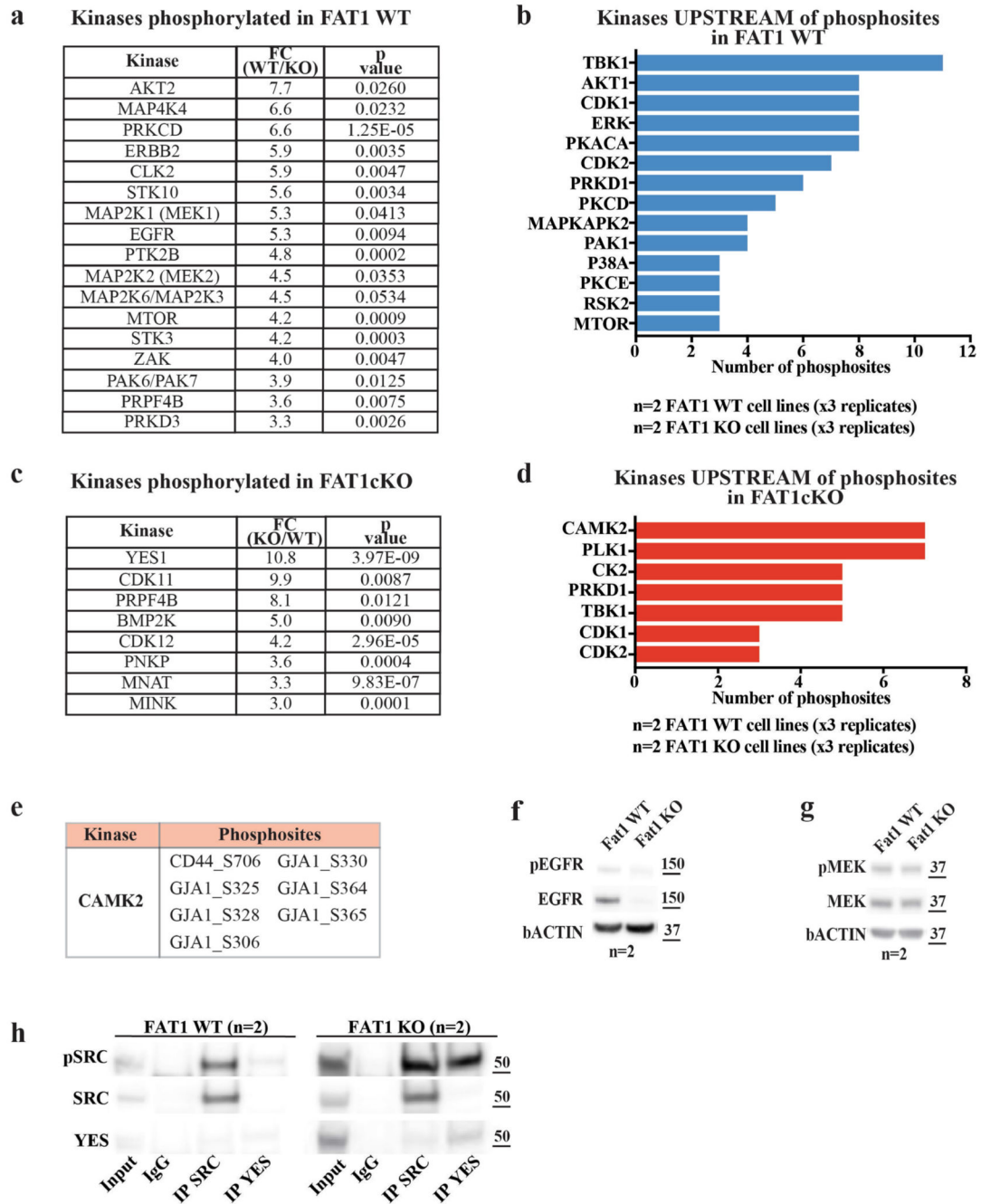
control tumour cells as determined by Homer. Cumulative hypergeometric distributions. White boxes show core transcription factors; boxes highlighted in green show epithelial transcription factors; and boxes highlighted in orange show EMT transcription factors. **d**, Transcription factor motifs enriched in the ATAC-seq peaks that are upregulated between the EPCAM⁻ *Fat1*-cKO and EPCAM⁻ control tumour cells as determined by Homer analysis. Cumulative hypergeometric distributions. White boxes show core transcription factors; boxes highlighted in green show epithelial transcription factors; boxes highlighted in orange show EMT transcription factors; and boxes highlighted in grey show other transcription factors. **e**, ATAC-seq of the chromatin regulatory regions of epithelial genes with open chromatin regions in EPCAM⁻ *Fat1*-cKO tumour cells as compared to EPCAM⁻ tumour cells from LGR5-derived SCCs, showing the sustained opening of epithelial enhancers in EPCAM⁻ *Fat1*-cKO tumour cells. **f**, ATAC-seq of the chromatin regulatory regions of epithelial genes that are closed upon EMT, irrespective of *Fat1* deletion. **g**, Immunostaining for GFP and AP2G, KLF4, SOX2, p63, GRHL2 or ZEB1 in EPCAM⁺ and EPCAM⁻ control and *Fat1*-cKO DMBA/TPA skin SCCs. Scale bar, 50 μm.



Extended Data Fig. 7. Loss of cell adhesion is not sufficient to induce the hybrid EMT phenotype.

a, Images showing spheroids formed 7 d after plating 4,000 *FAT1* wild-type or *FAT1* wild-type, *CDHI*-knockout human A388 skin SCC cells on an ultra-low adherent plate. **b**, Bar chart showing the quantification by FACS of the number of cells in *FAT1* wild-type, and *FAT1* wild-type and *CDHI*-knockout, spheroids. Mean + s.e.m., two-tailed *t*-test. **c**, Immunostaining for E-cadherin, YAP1, ZEB1 and SOX2 in *FAT1* wild-type, and *FAT1* wild-type and *CDHI*-knockout, tumour cells. Scale bar, 50 μ m. **d**, Images showing spheroids formed 7 d after plating 4,000 *FAT1*-knockout or *FAT1*-knockout and *CDHI*-overexpressing

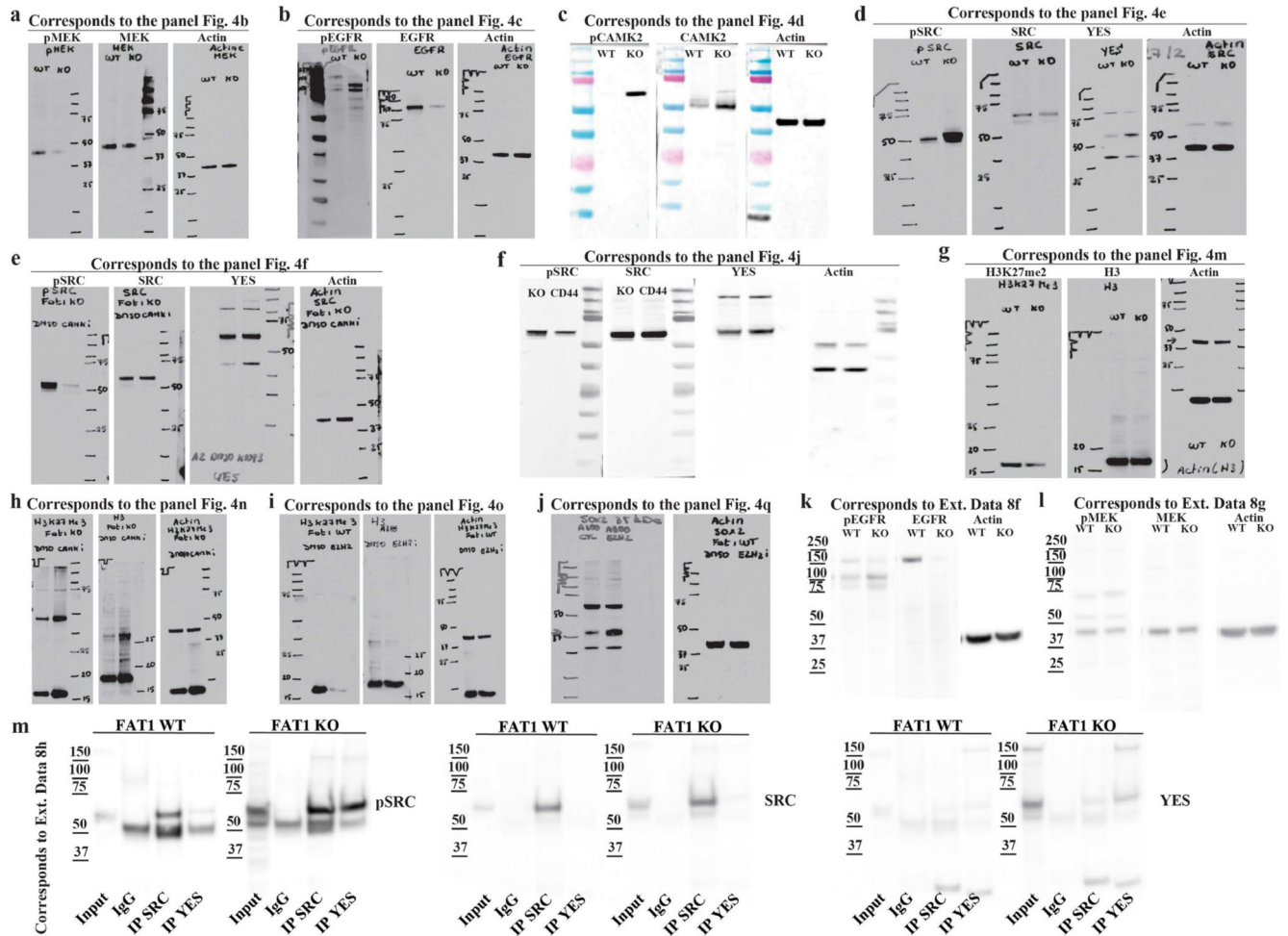
human A388 skin SCC cells on an ultra-low attachment plate. **e**, Bar chart showing the quantification by FACS of the number of cells in *FAT1*-knockout or *FAT1*-knockout and *CDH1*-overexpressing spheroids. Mean + s.e.m., two-tailed *t*-test. **f**, Immunostaining for E-cadherin, YAP1, ZEB1 and SOX2 in *FAT1*-knockout or *FAT1*-knockout and *CDH1*-overexpressing tumour cells. Scale bar, 50 μ m. **g–i**, Immunostaining of K14 and vimentin after subcutaneous transplantation of *Fat1*-cKO (**g**), *Fat1* and *Sox2* double-knockout (**h**) or *Fat1*, *Yap1* and *Taz* triple-knockout (**i**) mouse skin SCC cells. Mean \pm s.e.m. Scale bars, 50 μ m. **j**, **k**, Venn diagram of the genes upregulated in EPCAM⁻ *Fat1*-cKO skin SCC upon *Sox2* deletion (**j**) or upon *Yap1* and *Taz* deletion (**k**), and upregulated genes in hybrid EMT triple-negative cells versus late EMT triple-positive cells (early hybrid EMT signature) and in triple-positive versus EPCAM⁺ cells (late EMT signature). Two-sided hypergeometric test.



Extended Data Fig. 8. Phosphoproteomic analysis reveals signalling cascades downstream of *FAT1* LOF.

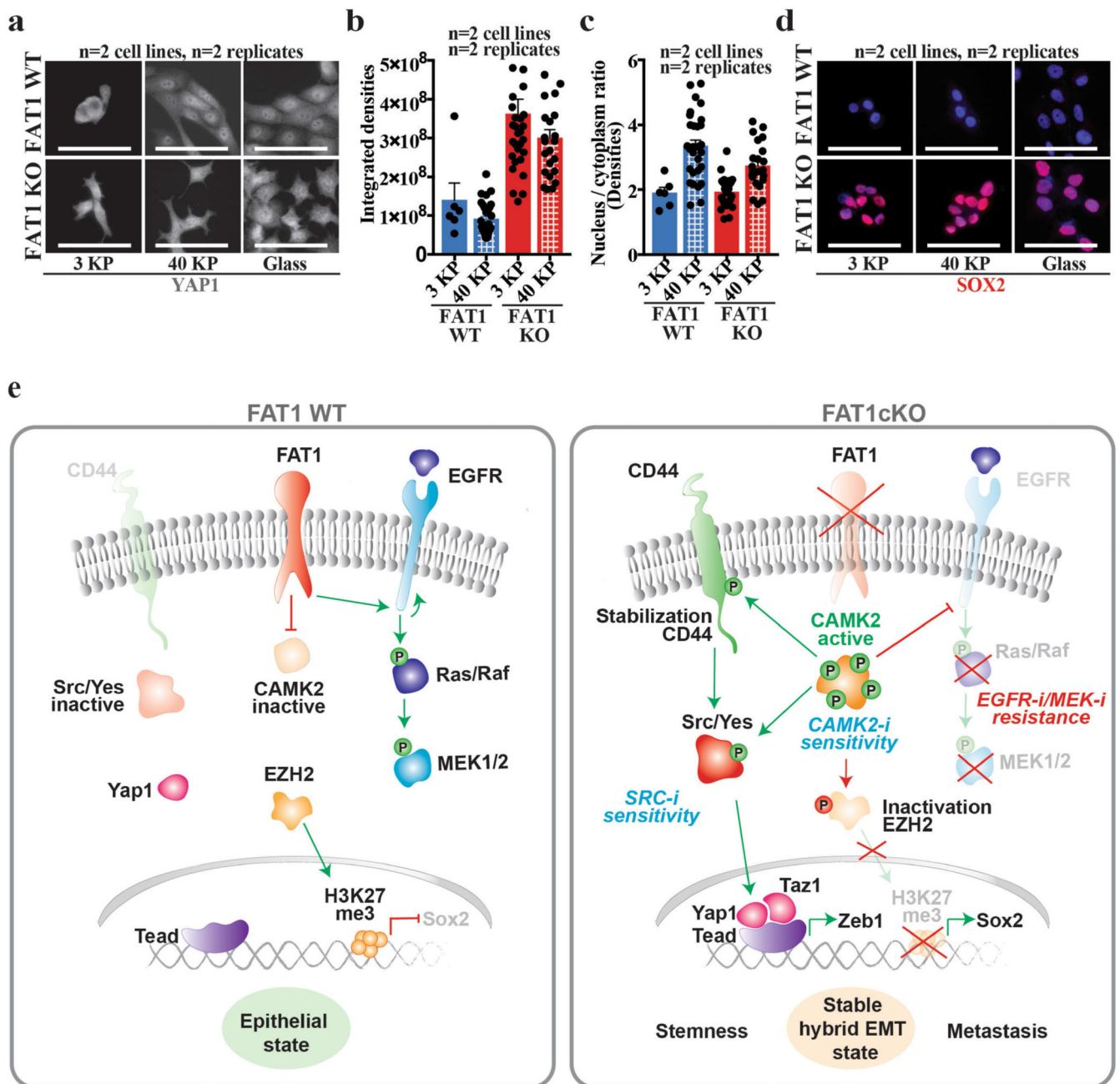
a, Table showing kinases that are significantly more phosphorylated in *FAT1* wild-type cells as compared to *FAT1*-knockout cells. *t*-test, FDR = 0.05, $S_0 = 1$. **b**, Bar chart showing the kinases that are predicted to phosphorylate phosphosites significantly enriched in *FAT1* wild-type tumour cells. **c**, Table showing kinases that are significantly more phosphorylated in *FAT1*-knockout cells as compared to *FAT1* wild-type cells. *t*-test, FDR = 0.05, $S_0 = 1$. **d**, Bar chart showing the kinases that are predicted to phosphorylate phosphosites that

are significantly enriched in *FAT1*-knockout tumour cells. **e**, Table showing the sites in *FAT1*-knockout cells predicted to be phosphorylated by CAMK2. **f, g**, Western blot showing pEGFR and EGFR (**f**) or pMEK and MEK (**g**) in *Fat1* wild-type and *Fat1*-knockout *Lgr5-creER;Kras^{G12D};p53^{co};*Fat1^{fl/fl};RYFP* mouse skin SCC cells. **h**, Western blot showing the expression levels of pSRC, total SRC and YES on the input of wild-type and *FAT1*-knockout cells, and upon immunoprecipitation of SRC and YES ($n = 4$). The apparent molecular weight reference in kDa is indicated close to **f-h**.*



Extended Data Fig. 9. Full scan of western blot membranes.

a-k, Images showing full scan of western blot membranes displayed in Fig. 4. Each panel indicates the figure and the panel to which the full membrane image belongs. Molecular weight size standards are indicated on each membrane. In all the experiments the controls (β -actin) were run on the same gel as the samples.



Extended Data Fig. 10. Increase in YAP1 and SOX2 signalling downstream of *FAT1* LOF is independent of the stiffness of the substrate.

a, Immunostaining for YAP1 in *FAT1* wild-type and *FAT1*-knockout human SCC cells upon increasing stiffness conditions. Scale bar, 50 μ m. **b**, Quantification of YAP1 expression on the basis of fluorescence intensity in *FAT1* wild-type and *FAT1*-knockout cells in different stiffness conditions. Mean + s.e.m. **c**, Quantification of YAP1 nuclear/cytoplasmic ratio on the basis of fluorescence intensity in *FAT1* wild-type and *FAT1*-knockout cells in different stiffness conditions. Mean + s.e.m. **d**, Immunostaining for SOX2 in *FAT1* wild-type and *FAT1*-knockout human SCC cells in increasing stiffness conditions. Scale bar, 50 μ m **e**,

Model of the signalling pathways that are activated or repressed in *FAT1*-knockout cells to induce a hybrid EMT state and to predict a differential effect on the response to therapy.

Supplementary Material

Refer to Web version on PubMed Central for supplementary material.

Acknowledgements

We thank the ULB animal facility and ULB genomic core facility (F. Libert and A. Lefort); and J. Allard from CMMI (supported by the European Regional Development Fund and the Walloon Region). I.P. is supported by FNRS and Foundation Against Cancer (FCC). F.M. was supported by FNRS post-doctoral fellowship and by the TELEVIE. The Department of Pathology (Erasmé Hospital, ULB) acknowledges Fonds Yvonne Boel. C. Decaestecker is a senior research associate in F.R.S.-FNRS. The patient-derived xenograft project was supported by Fonds Erasme. C. Blanpain is supported by WELBIO, FNRS, Fond Erasme, Fondation Contre le Cancer, ULB Foundation, European Research Council, Worldwide Cancer Research and the Foundation Baillet Latour.

Data availability

All the raw sequencing data have been deposited in the Gene Expression Omnibus with the following accession numbers: mouse RNA-seq (GSE158502), human RNA-seq (GSE158501), ATAC-seq (GSE158501), whole-exome sequencing (GSE158503), low-coverage whole-genome sequencing (GSE158505) or a global accession number (GSE158506). The mass spectrometry proteomics data have been deposited to the ProteomeXchange Consortium via the PRIDE partner repository with the dataset identifier PXD022268. All other relevant data are available from the corresponding author upon reasonable request. Source data are provided with this paper.

References

1. Morris LG, et al. Recurrent somatic mutation of *FAT1* in multiple human cancers leads to aberrant Wnt activation. *Nat Genet.* 2013; 45: 253–261. [PubMed: 23354438]
2. Dotto GP, Rustgi AK. Squamous cell cancers: a unified perspective on biology and genetics. *Cancer Cell.* 2016; 29: 622–637. [PubMed: 27165741]
3. Sánchez-Danés A, Blanpain C. Deciphering the cells of origin of squamous cell carcinomas. *Nat Rev Cancer.* 2018; 18: 549–561. [PubMed: 29849070]
4. The ICGC/TCGA Pan-Cancer Analysis of Whole Genomes Consortium. Pan-cancer analysis of whole genomes. *Nature.* 2020; 578: 82–93. [PubMed: 32025007]
5. Lawrence MS, et al. Discovery and saturation analysis of cancer genes across 21 tumour types. *Nature.* 2014; 505: 495–501. [PubMed: 24390350]
6. Li Z, et al. Loss of the *FAT1* tumor suppressor promotes resistance to CDK4/6 inhibitors via the Hippo pathway. *Cancer Cell.* 2018; 34: 893–905. e8 [PubMed: 30537512]
7. Nassar D, Latil M, Boeckx B, Lambrechts D, Blanpain C. Genomic landscape of carcinogen-induced and genetically induced mouse skin squamous cell carcinoma. *Nat Med.* 2015; 21: 946–954. [PubMed: 26168291]
8. Martin D, et al. Assembly and activation of the Hippo signalome by *FAT1* tumor suppressor. *Nat Commun.* 2018; 9: 2372 [PubMed: 29985391]
9. Hu X, et al. *FAT1* prevents epithelial mesenchymal transition (EMT) via MAPK/ERK signaling pathway in esophageal squamous cell cancer. *Cancer Lett.* 2017; 397: 83–93. [PubMed: 28366557]
10. Srivastava C, et al. *FAT1* modulates EMT and stemness genes expression in hypoxic glioblastoma. *Int J Cancer.* 2018; 142: 805–812. [PubMed: 28994107]

11. Pastushenko I, et al. Identification of the tumour transition states occurring during EMT. *Nature*. 2018; 556: 463–468. [PubMed: 29670281]
12. Latil M, et al. Cell-type-specific chromatin states differentially prime squamous cell carcinoma tumor-initiating cells for epithelial to mesenchymal transition. *Cell Stem Cell*. 2017; 20: 191–204. e5 [PubMed: 27889319]
13. Pastushenko I, Blanpain C. EMT transition states during tumor progression and metastasis. *Trends Cell Biol*. 2019; 29: 212–226. [PubMed: 30594349]
14. Nieto MA, Huang RY, Jackson RA, Thiery JP. EMT: 2016. *Cell*. 2016; 166: 21–45. [PubMed: 27368099]
15. Boumahdi S, et al. SOX2 controls tumour initiation and cancer stem-cell functions in squamous-cell carcinoma. *Nature*. 2014; 511: 246–250. [PubMed: 24909994]
16. Ferone G, et al. SOX2 is the determining oncogenic switch in promoting lung squamous cell carcinoma from different cells of origin. *Cancer Cell*. 2016; 30: 519–532. [PubMed: 27728803]
17. Siegle JM, et al. SOX2 is a cancer-specific regulator of tumour initiating potential in cutaneous squamous cell carcinoma. *Nat Commun*. 2014; 5 4511 [PubMed: 25077433]
18. Cooper CD, Lampe PD. Casein kinase 1 regulates connexin-43 gap junction assembly. *J Biol Chem*. 2002; 277: 44962–44968. [PubMed: 12270943]
19. Lewis CA, Townsend PA, Isacke CM. Ca²⁺/calmodulin-dependent protein kinase mediates the phosphorylation of CD44 required for cell migration on hyaluronan. *Biochem J*. 2001; 357: 843–850. [PubMed: 11463356]
20. Huang RY, et al. Identification of CaMKII phosphorylation sites in connexin43 by high-resolution mass spectrometry. *J Proteome Res*. 2011; 10: 1098–1109. [PubMed: 21158428]
21. Chen C, Zhao S, Karnad A, Freeman JW. The biology and role of CD44 in cancer progression: therapeutic implications. *J Hematol Oncol*. 2018; 11 64 [PubMed: 29747682]
22. Jolly MK, et al. Interconnected feedback loops among ESRP1, HAS2, and CD44 regulate epithelial-mesenchymal plasticity in cancer. *APL Bioeng*. 2018; 2 031908 [PubMed: 31069317]
23. Chellaiah MA, Biswas RS, Rittling SR, Denhardt DT, Hruska KA. Rho-dependent Rho kinase activation increases CD44 surface expression and bone resorption in osteoclasts. *J Biol Chem*. 2003; 278: 29086–29097. [PubMed: 12730217]
24. Göllner S, et al. Loss of the histone methyltransferase EZH2 induces resistance to multiple drugs in acute myeloid leukemia. *Nat Med*. 2017; 23: 69–78. [PubMed: 27941792]
25. Avgustinova A, Benitah SA. Epigenetic control of adult stem cell function. *Nat Rev Mol Cell Biol*. 2016; 17: 643–658. [PubMed: 27405257]
26. Panciera T, Azzolin L, Cordenonsi M, Piccolo S. Mechanobiology of YAP and TAZ in physiology and disease. *Nat Rev Mol Cell Biol*. 2017; 18: 758–770. [PubMed: 28951564]
27. Machiels JP, et al. Afatinib versus methotrexate as second-line treatment in patients with recurrent or metastatic squamous-cell carcinoma of the head and neck progressing on or after platinum-based therapy (LUX-Head & Neck 1): an open-label, randomised phase 3 trial. *Lancet Oncol*. 2015; 16: 583–594. [PubMed: 25892145]
28. Planchard D, et al. Dabrafenib plus trametinib in patients with previously untreated BRAF^{V600E}-mutant metastatic non-small-cell lung cancer: an open-label, phase 2 trial. *Lancet Oncol*. 2017; 18: 1307–1316. [PubMed: 28919011]

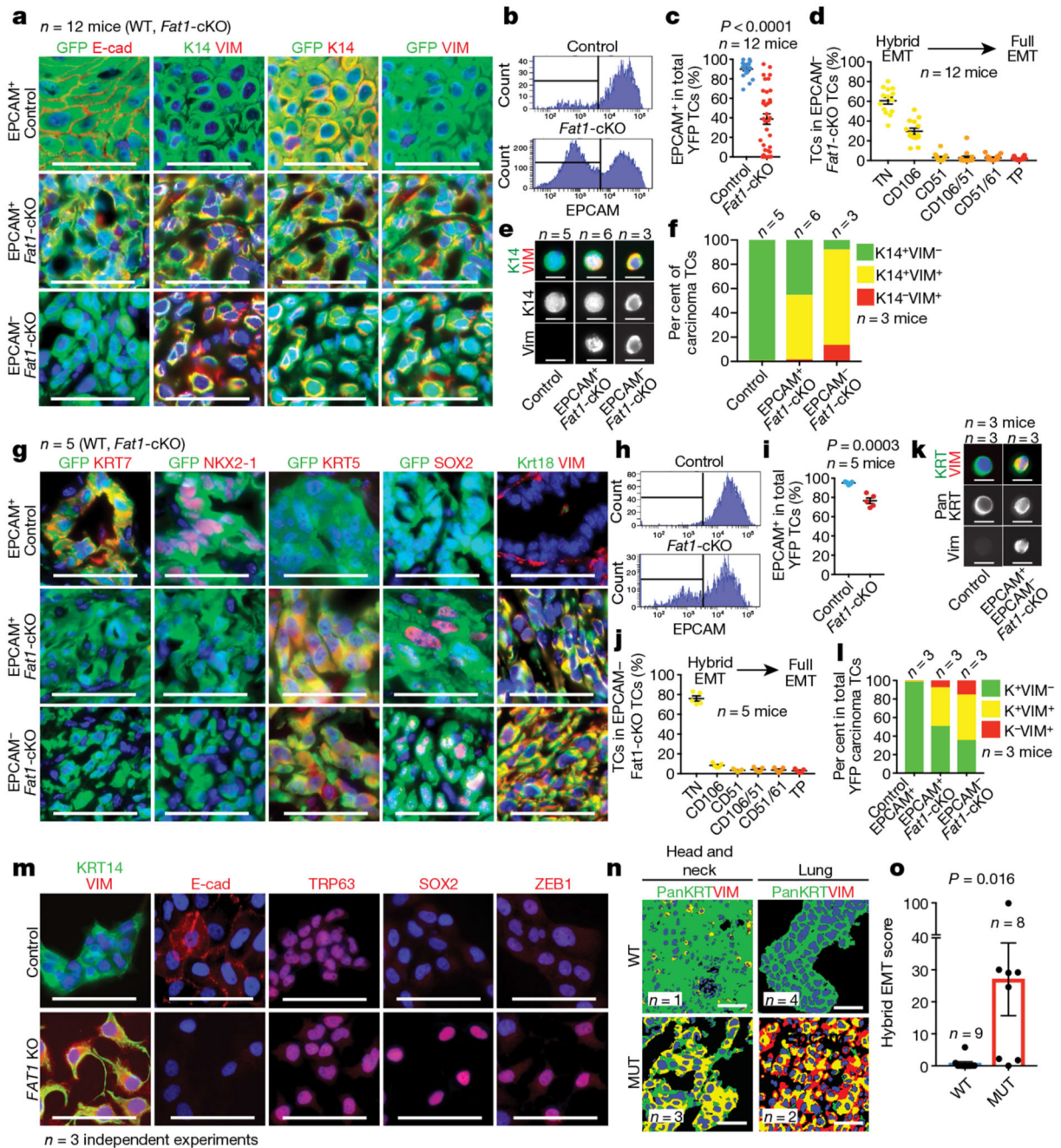


Fig. 1. LOF of *Fat1* promotes hybrid EMT state in mouse skin SCC, mouse lung cancer and human SCC.

a. Immunostaining for GFP, E-cadherin (E-cad), vimentin (VIM) and KRT14 (K14) in EPCAM⁺ control (wild-type (WT)), EPCAM⁺ *Fat1*-cKO and EPCAM⁻ *Fat1*-cKO DMBA/TPA-induced SCCs. Scale bars, 50 μm. **b, c.** FACS analysis (**b**) and percentage of EPCAM expression (**c**) in control and *Fat1*-cKO YFP⁺ skin SCCs. Mean ± s.e.m., two-tailed *t*-test. TC, tumour cell. **d.** Distribution of YFP⁺EPCAM⁻ tumour cells in CD106 (also known as VCAM1), CD61 (also known as ITGB3) and CD51 (also known as ITGAV) subpopulations

in *Fat1*-cKO SCCs. Mean \pm s.e.m. TN, EPCAM⁻ triple negative (CD106⁻CD51⁻CD61⁻); TP, EPCAM⁻ triple positive (CD106⁺CD51⁺CD61⁺). **e, f**, Co-immunostaining (**e**) and quantification (**f**) of KRT14 and vimentin in cytospin of FACS-isolated skin SCC tumour cells. Scale bars, 20 μ m. $n = 90$ cells per condition and tumour. **g**, Immunostaining for GFP, KRT7, NKX2-1, KRT5, SOX2, KRT8 and KRT18 (KRT8/18), and vimentin in *Fat1* wild-type and -knockout lung carcinomas. Scale bars, 50 μ m. **h, i**, FACS analysis (**h**) and percentage of EPCAM expression (**i**) in control and *Fat1*-cKO YFP⁺ lung tumour cells. Mean \pm s.e.m., two-tailed *t*-test. **j**, Distribution of YFP⁺EPCAM⁻ tumour cells in CD106/VCAM1, CD61/ITGB3 and CD51/ITGAV subpopulations in *Fat1*-cKO lung carcinomas. Mean \pm s.e.m. **k, l**, Co-immunostaining (**k**) and quantification (**l**) of pancytokeratin (pan KRT) and vimentin in cytospin of FACS-isolated lung carcinoma tumour cells. Scale bars, 20 μ m. $n = 70$ cells per condition and tumour. In **l**, K denotes pancytokeratin. **m**, Immunostaining for KRT14 and vimentin, E-cadherin, SOX2, TRP63 and ZEB1 in *FAT1* wild-type and *FAT1*-knockout (KO) A388 human skin SCC cell line. Scale bars, 50 μ m. **n, o**, Representative images (**n**) and quantification of hybrid EMT score (**o**) (colocalization of pancytokeratin and vimentin) in wild-type and *FAT1*-mutated (MUT) head and neck, and lung, patient-derived xenografts. Scale bars, 50 μ m, Mean \pm s.e.m., two-tailed Mann-Whitney *U* test.

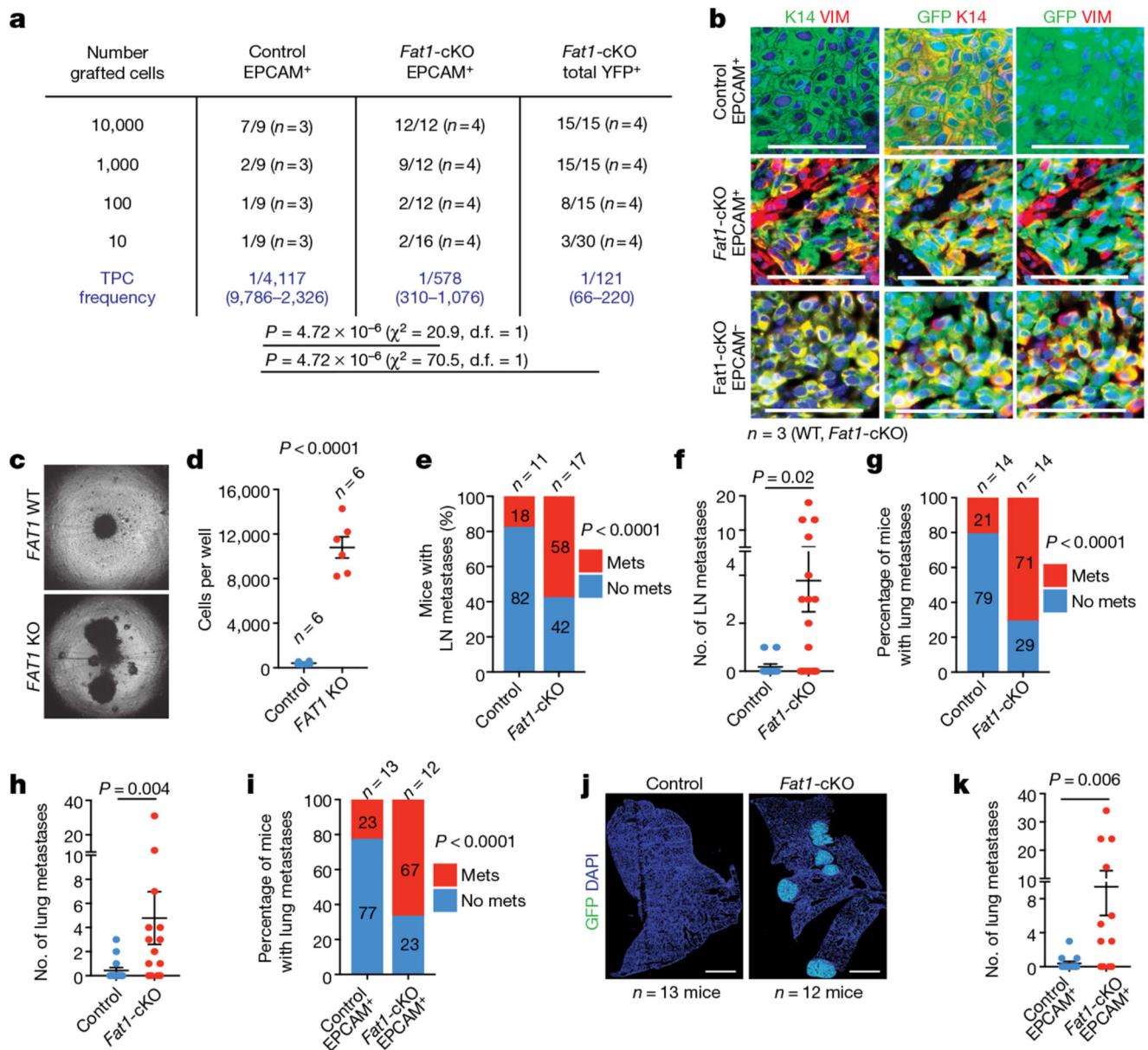


Fig. 2. *Fat1* deletion promotes tumour stemness and metastasis in skin SCCs.

a, Tumour-propagating cell (TPC) frequency observed upon subcutaneous transplantation of limiting dilutions of YFP⁺EPCAM⁺ control, YFP⁺EPCAM⁺ and total YFP⁺ *Fat1*-cKO tumour cells using extreme limiting dilution analysis. χ^2 test. d.f., degrees of freedom.

b, Immunostaining for GFP, KRT14 and vimentin in the secondary tumours arising after subcutaneous transplantation of tumour cells. Scale bars, 50 μ m. **c**, Images showing spheroids formed 7 d after plating 4,000 *FAT1* wild-type or *FAT1*-knockout human A388 skin SCC cells on an ultra-low adherent plate.

d, Quantification of cell number in *FAT1* wild-type and *FAT1*-knockout spheroids. Mean \pm s.e.m., two-tailed *t*-test. **e**, **f**, Proportion of mice presenting lymph node (LN) metastasis (χ^2 test) (**e**) and number of lymph node metastases per mouse (**f**) (mean \pm s.e.m., two-tailed *t*-test). Mets, metastases. **g**, **h**,

Proportion of mice presenting lung metastasis (χ^2 test) (**g**) and number of lung metastases per mouse (**h**) (mean \pm s.e.m., two-tailed *t*-test). **i**, Proportion of mice presenting lung metastasis 40 d after intravenous injection of 20,000 YFP⁺EPCAM⁺ tumour cells. χ^2 test. **j**, Mosaic images of immunostaining for YFP of lungs after intravenous injection of control and *Fat1*-cKO tumour cells Scale bars, 1 mm. **k**, Number of metastases per lung arising from the injection of 20,000 YFP⁺EPCAM⁺ *Fat1* wild-type and *Fat1*-cKO tumour cells. Mean \pm s.e.m., two-tailed *t*-test.

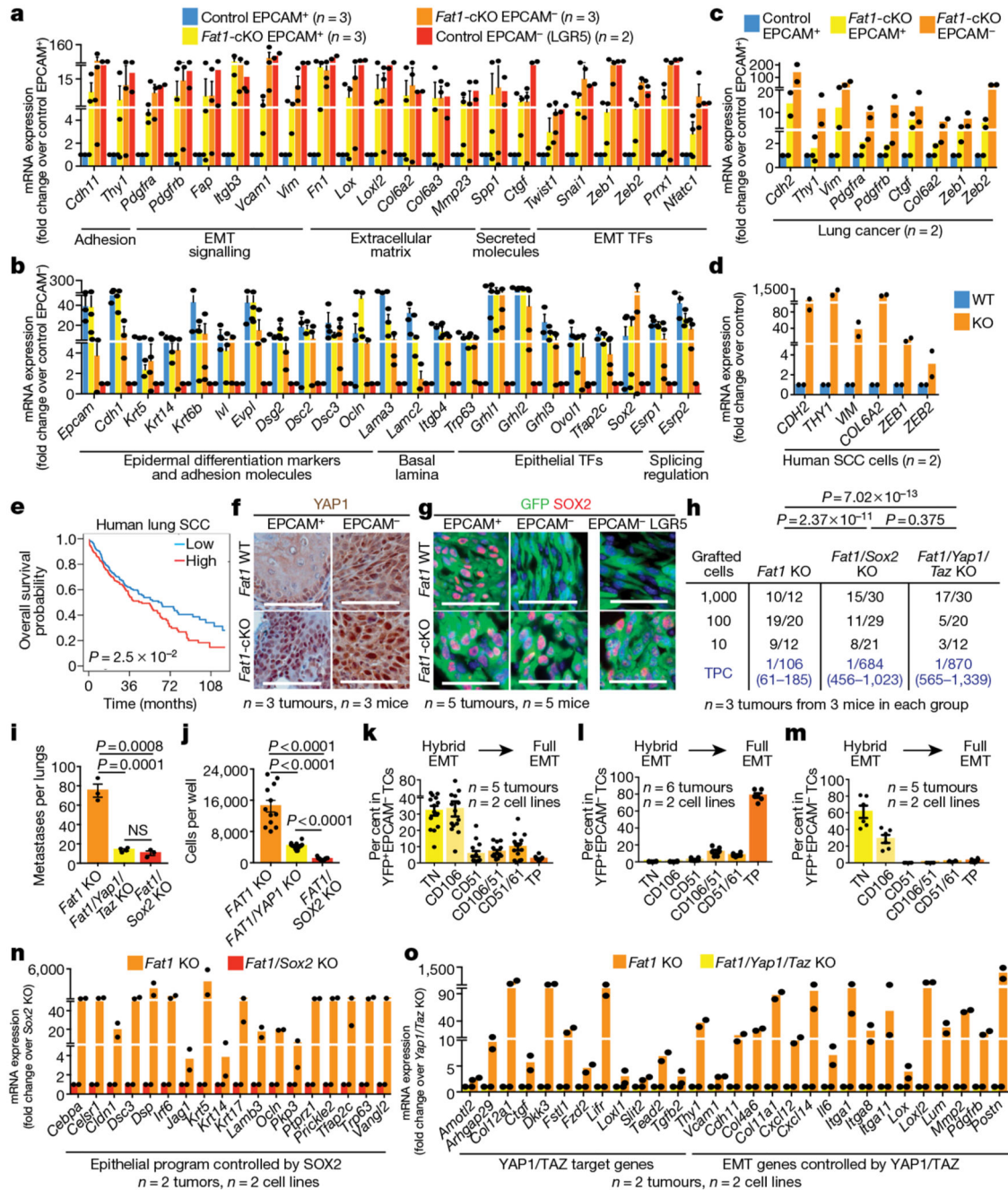


Fig. 3. YAP1 and SOX2 regulate mesenchymal and epithelial states downstream of Fat1 deletion.

a, b, mRNA expression (RNA-seq) of mesenchymal (**a**) and epithelial (**b**) genes in mouse skin SCC. Mean + s.e.m. TF, transcription factor. **c, d**, mRNA expression (RNA-seq) of mesenchymal genes in mouse lung carcinoma (**c**) and human SCC cells (**d**). Mean + s.e.m. **e**, Overall survival of patients with lung SCC, stratified by the expression of the common gene signature between mouse skin and lung and human skin FAT1-knockout SCC. log-rank Mantel-Cox test. **f, g**, Immunohistochemistry for YAP1 (**f**) and immunostaining for GFP and SOX2 (**g**) in wild-type and Fat1-cKO skin SCCs. Scale bars, 50 μ m. **h, i**, Tumour-

propagating cells (**h**) and lung metastasis (**i**) following the injection of YFP⁺EPCAM⁻ *Fat1*-knockout, *Fat1*- and *Sox2* double-knockout or *Fat1*, *Yap1* and *Taz* triple-knockout skin SCC cells. Mean \pm s.e.m. two-tailed-*t*-test. NS, not significant. **j**, Number of cells in spheroids formed by *FAT1*-knockout, *FAT1* and *YAP1* double-knockout or *FAT1* and *SOX2* double-knockout human SCC cells after 7 d. Mean \pm s.e.m., two-tailed *t*-test. **k–m**, YFP⁺EPCAM⁻ CD106/VCAM1, CD61/ITGB3 and CD51/ITGAV subpopulations in SCC after subcutaneous transplantation of *Fat1*-cKO (**k**), *Fat1* and *Sox2* double-knockout (**l**) or *Fat1*, *Yap1* and *Taz* triple-knockout (**m**) mouse skin SCC cells. Mean \pm s.e.m. Scale bars, 50 μ m. **n, o**, mRNA (RNA-seq) expression of genes controlled by *Sox2* (**n**) or by *Yap1* and *Taz* (**o**) in EPCAM⁻ *Fat1*-cKO skin SCC. Mean \pm s.e.m.

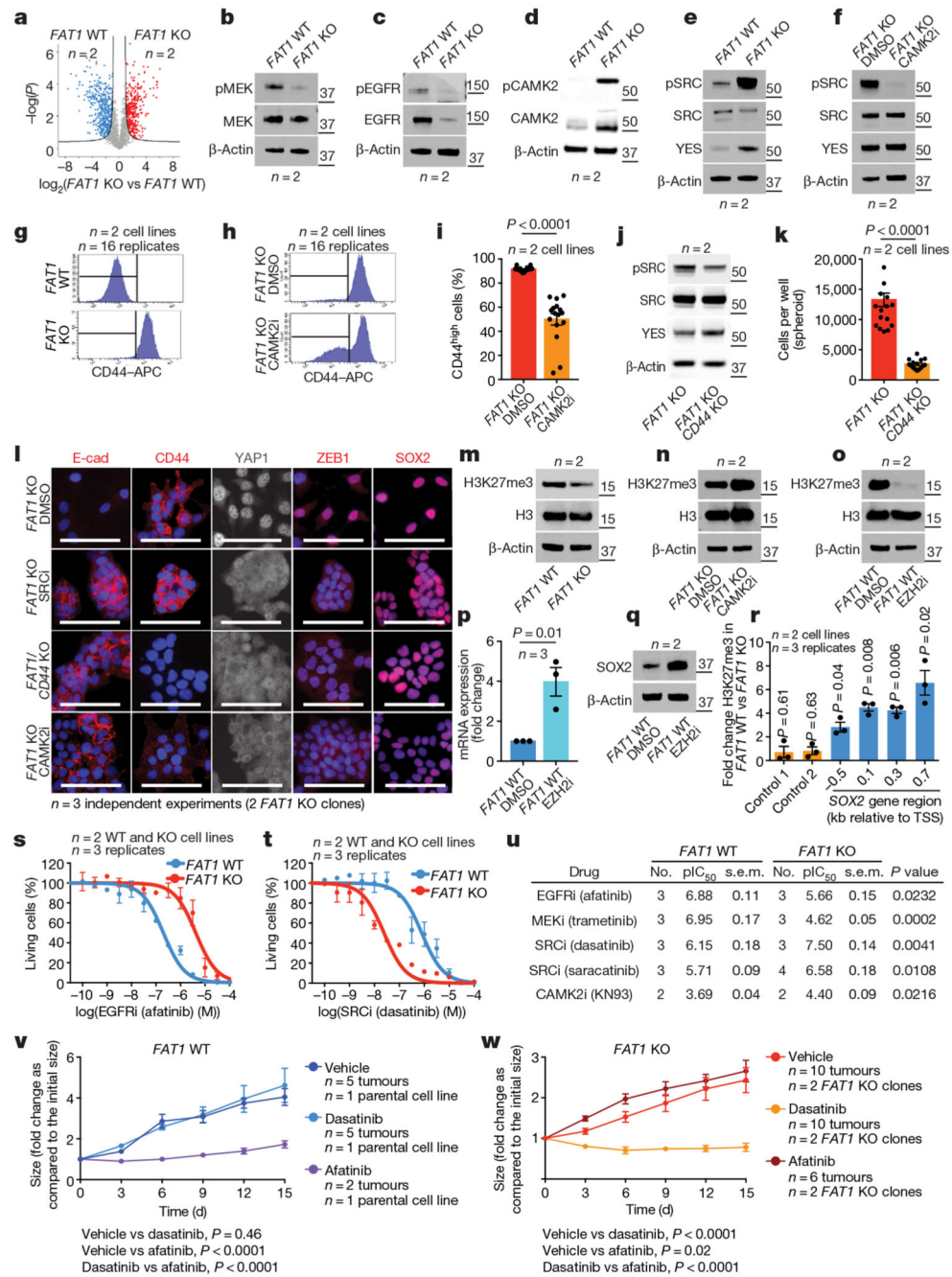


Fig. 4. Phosphoproteomic analysis identifies the signalling cascades downstream of *FAT1* deletion.

a, Volcano plot showing the fold change and statistical significance of each phosphopeptide in wild-type versus *FAT1*-knockout cells (false-discovery rate (FDR) = 0.05, $S_0 = 1$).

b–e, Western blot showing phosphorylated (p)MEK1 and MEK2 (MEK1/2) and total MEK (**b**), pEGFR and total EGFR (**c**), pCAMK2 and total CAMK2 (**d**), and pSRC, total SRC and YES (**e**) in *FAT1*-knockout and wild-type cells. **f**, Western blot showing pSRC, total SRC and YES in *FAT1*-knockout cells treated with dimethyl sulfoxide (DMSO) or with a

CAMK2 inhibitor (CAMK2i). **g, h**, FACS analysis showing CD44 expression in wild-type and *FAT1*-knockout cells (**g**), and in *FAT1*-knockout cells treated with a CAMK2 inhibitor (**h**). **i**, *FAT1*-knockout cells expressing high levels of CD44 were treated with DMSO or a CAMK2 inhibitor. Mean + s.e.m. two-tailed-*t*-test. **j**, Western blot showing pSRC, total SRC and YES in *FAT1*-knockout and *FAT1* and *CD44* double-knockout cells. **k**, Number of cells in *FAT1*-knockout and *FAT1* and *CD44* double-knockout spheroids. Mean + s.e.m. two-tailed-*t*-test. **l**, Immunostaining for E-cadherin, CD44, YAP1, ZEB1 and SOX2 in *FAT1* and *CD44* double-knockout, and *FAT1*-knockout, cells treated with DMSO, an SRC inhibitor (SRCi) (saracatinib) or a CAMK2 inhibitor. Scale bars, 50 μ m. **m–o**, Western blot showing the expression of H3K27me3 and total H3 in *FAT1* wild-type and -knockout cells (**m**), *FAT1*-knockout cells treated with a CAMK2 inhibitor (**n**) and in *FAT1* wild-type cells treated with DMSO or an EZH2 inhibitor (EZH2i) (**o**). **p, q**, *SOX2* mRNA (quantitative PCR with reverse transcription) (**p**) and protein (western blot) (**q**) in *FAT1* wild-type cells 7 d after treatment with an EZH2 inhibitor. Mean \pm s.e.m., two-tailed *t*-test. **r**, CHIP-qPCR of H3K27me3 mark in regions close to the *SOX2* transcription start site. Ratio of relative enrichment in *FAT1* wild-type versus -knockout cells; one sample *t*-test, mean \pm s.e.m. **s, t**, Dose–response curve showing the effect of the EGFR inhibitor (ECFRi) afatinib (**s**) and the SRC inhibitor dasatinib (**t**) on *FAT1* wild-type and *FAT1*-knockout cell viability at 48 h. Nonlinear regression log (inhibitor) with least-squares fit method. Mean \pm s.e.m. **u**, Summary ($n = 3$) of pIC₅₀ (negative log of half-maximal inhibitor concentration) and s.e.m. for different drugs for *FAT1* wild-type and *FAT1*-knockout cells. Two-tailed *t*-test. **v, w**, Effect of dasatinib and afatinib on *FAT1* wild-type (**v**) and *FAT1*-knockout (**w**) tumour growth upon subcutaneous transplantation. Mean \pm s.e.m., two-way analysis of variance. The molecular weight (kDa) is indicated to the right of the blots in **b–f, j, m–o, q**.